

Direct *circMAN1A2(2,3,4,5)*-*CENPB* mRNA interaction regulates cell proliferation and cancer progression

Received: 17 October 2024

Accepted: 26 August 2025

Published online: 29 September 2025

 Check for updatesMei Cao ^{1,7}, Guo-Hua Yuan ^{2,7}, Shi-Meng Cao ^{3,7}, Yu-Xin Liu³,
Chu-Xiao Liu ³, Yi-Feng Xu ³, Jia Wei¹, Yi-Lin Guo¹, Ling-Ling Chen ^{3,4,5,6} &
Li Yang ¹ ✉

Numerous covalently closed circular RNAs (circRNAs) are produced from back-splicing of eukaryotic exons, and multiple circRNAs can be generated from a single gene locus through alternative circularization (AC). However, functions of most AC circRNAs remain poorly understood. Here, we profile the landscape of AC across multiple cell lines and colorectal cancer (CRC) tissues, identifying predominantly expressed circRNAs (pe-circRNA) in each AC gene locus. Other than cell-type-specific expression of most top pe-circRNAs, *circMAN1A2(2,3,4,5)*, a universally expressed pe-circRNA in examined samples, plays an important role in cell proliferation and CRC progression. Mechanistically, *circMAN1A2(2,3,4,5)* directly interacts with the 3' untranslated region of Centromere Protein B (*CENPB*) mRNA via its characteristic back-splicing junction site, which enhances IGF2BP2-mediated *CENPB* mRNA stability. Inhibition of *circMAN1A2(2,3,4,5)* expression with locked nucleic acids represses CRC progression. These results uncover the prevalence of AC and the regulatory role of a specific AC circRNA, *circMAN1A2(2,3,4,5)*, in cell proliferation and tumor progression.

Despite being lowly processed by the canonical spliceosomal machinery, back-splicing of pre-mRNA exons results in the genome-wide expression of circular RNAs (circRNAs) with nearly identical sequences to their cognate linear RNAs from the same gene loci, except those at their back-splicing junction (BSJ) sites^{1,2}. Importantly, increasing lines of evidence have shown that some circRNAs play important roles in gene expression regulation through different molecular modes of action^{3–5}. These include modulating transcription^{6,7}, interfering with mRNA splicing⁸, sponging microRNAs

or proteins^{9–12}, impacting translation^{13–15}, and being translated to produce peptides^{13,14,16}. Consequently, some highly expressed circRNAs have been involved in maintaining quiescent hematopoietic stem cells¹², regulating cell growth and cancer progression^{13,17–19}, impacting brain function and neuronal development^{20,21}, and modulating innate immune responses^{22,23}. These findings thus expand the complexity and diversity of the human transcriptome.

The functional complexity of circRNAs is further expanded by alternative circularization (AC), which results in the production of

¹Center for Molecular Medicine, Children's Hospital of Fudan University and Shanghai Key Laboratory of Medical Epigenetics, International Laboratory of Medical Epigenetics and Metabolism, Ministry of Science and Technology, Institutes of Biomedical Sciences, Fudan University, Shanghai, China. ²Shanghai Institute of Nutrition and Health, University of Chinese Academy of Sciences, Chinese Academy of Sciences, Shanghai, China. ³State Key Laboratory of RNA Innovation, Science and Engineering, New Cornerstone Science Laboratory, CAS Center for Excellence in Molecular Cell Science, Shanghai Institute of Biochemistry and Cell Biology, University of Chinese Academy of Sciences, Chinese Academy of Sciences, Shanghai, China. ⁴School of Life Science and Biotechnology, Shanghai Jiao Tong University, Shanghai, China. ⁵School of Life Science and Technology, ShanghaiTech University, Shanghai, China. ⁶Shanghai Academy of Natural Sciences (SANS), Shanghai, China. ⁷These authors contributed equally: Mei Cao, Guo-Hua Yuan, Shi-Meng Cao.

✉ e-mail: liyong_fudan@fudan.edu.cn

multiple circRNAs from a single gene locus (Fig. 1a)^{24,25}. Diverse AC, including both alternative back-splicing and alternative splicing within back-spliced exons, contributes to the distinct landscapes of circRNA expression across different cell lines and tissues²⁵. With a common nomenclature, distinct circRNAs produced by AC from the same gene loci can be distinguished from each other by including their specific exonic (and intronic, if any) components²⁶.

Despite these advances, the understanding of how AC reshapes circRNA expression landscape and functional diversity has remained largely unexplored. More specifically, although circRNAs exhibit different expression patterns overall, can some highly expressed circRNAs produced via AC be universally identified across various cell lines and tissues, and if so, what are their biological roles? The ever-growing deep sequence datasets^{27,28} across different cell lines and

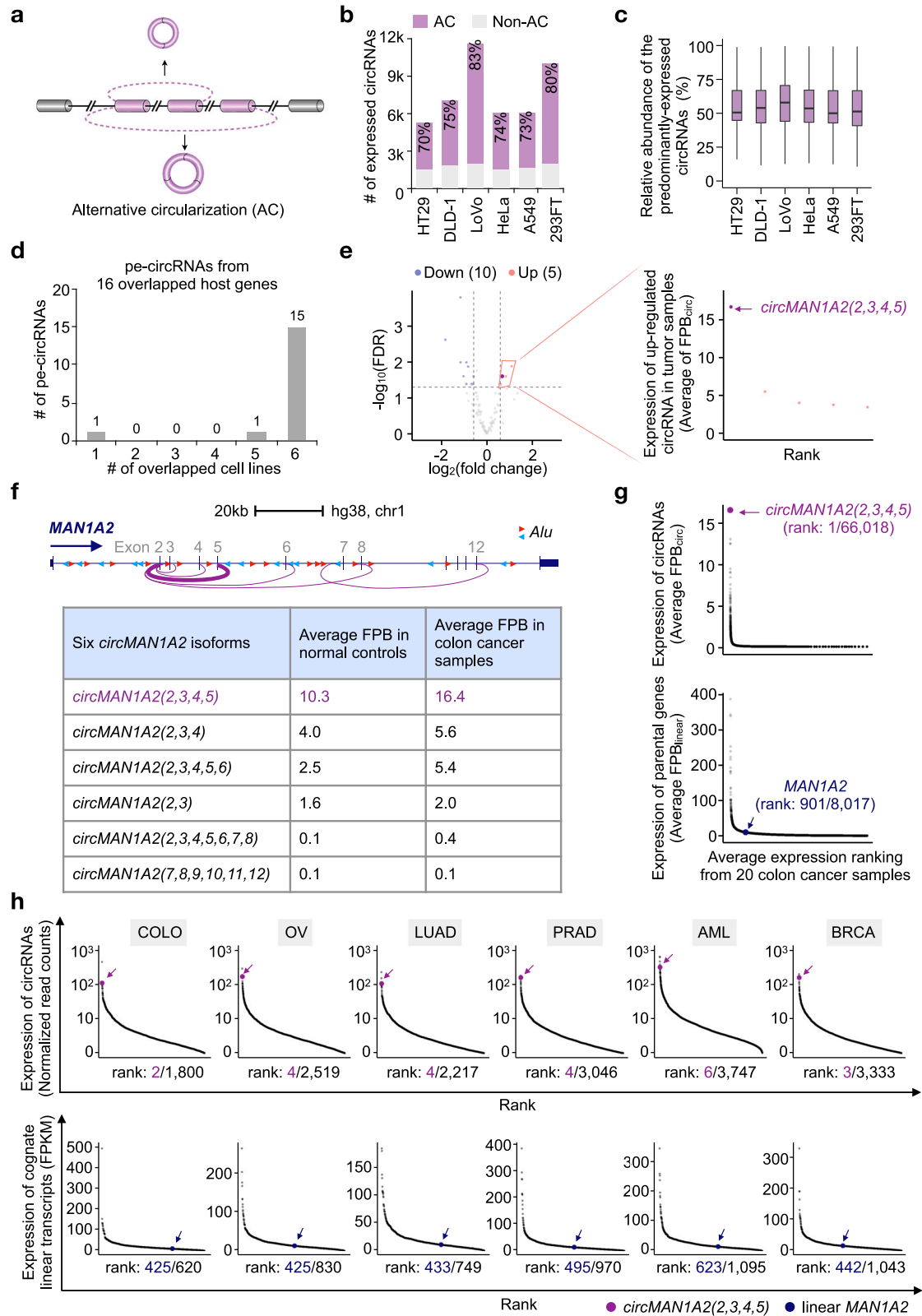


Fig. 1 | Profiling the alternative circularization to identify predominantly expressed *circMANIA2(2,3,4,5)*. **a** Schematic of alternative circularization (AC) in human transcriptome. **b** Numbers and percentages of total circRNAs with or without alternative circularization across various cell lines, including HT29, DLD-1, LoVo, HeLa, A549 and 293FT. **c** Relative abundance of the predominantly expressed circRNAs compared to all circRNAs derived from the same gene locus in examined cell lines. Box plots show the median (center line) and interquartile range (IQR; box), with whiskers extending to the most extreme data points within $1.5 \times$ IQR from the quartiles. RNA-seq was performed in each cell line with two biological replicates. **d** Overlapped predominantly expressed circRNAs from 16 host genes expressed in all six cell lines. **e** Volcano plot of differentially expressed circRNAs between normal and colorectal cancer samples among the top 100 predominantly expressed circRNAs. Five significantly upregulated predominantly expressed circRNAs in colorectal cancer samples were ranked by their absolute expression level (right panel). Results shown in (b–e) were derived from

ribo- RNA-seq data in GEO under the accession code GSE274247. **f** Schematic and expression of six confident *circMANIA2* isoforms detected in both normal and colorectal cancer samples. *Alu* elements with distinct orientations in flanking introns are highlighted by triangles with colors. **g** Expression rank of all identified circRNAs and their corresponding parental genes in the 20 colon cancer samples. Predominantly expressed *circMANIA2(2,3,4,5)* and its cognate *MANIA2* mRNA were highlighted. Results shown in (f and g) were obtained from publicly available paired ribo- RNA-seq data of normal and colon cancer patient samples³⁰, in GSA-Human under accession number PRJCA001113 upon request. **h** Expression rank of all alternative circularized circRNAs and their corresponding parental genes across various cancer tissues, including COLO, OV, LUAD, PRAD, AML, and BRCA. Predominantly expressed *circMANIA2(2,3,4,5)* and its cognate *MANIA2* mRNA were highlighted. Results shown in the (h) were obtained from publicly available exome capture RNA-seq data in the MiOncoCirc database³⁹.

tissues provide a basis for extensively identifying alternatively circularized circRNAs.

In this study, we profile the landscape of alternative circularized circRNAs across multiple cell lines as well as paired normal and colon cancer tissues. Although most AC events show a specific pattern in examined samples, we identify universally expressed *circMANIA2(2,3,4,5)* produced by AC at the *MANIA2* gene locus. Importantly, loss of *circMANIA2(2,3,4,5)* lead to retarded colorectal cancer (CRC) cell proliferation and tumor progression. Further analyses show that *circMANIA2(2,3,4,5)* can directly bind with *CENPB* mRNA via its unique BSJ sequence, and this impacts the IGF2BP2-mediated *CENPB* mRNA stability. Finally, a specific locked nucleic acid (LNA) targeting the BSJ of *circMANIA2(2,3,4,5)* in xenograft tumor models inhibits CRC progression, suggesting the importance of the direct *circMANIA2(2,3,4,5)*-*CENPB* mRNA interaction on cell proliferation and tumor progression.

Results

Profiling the alternative circularization landscape to identify predominantly expressed circRNAs

Multiple circRNAs can be produced from a single gene locus (Fig. 1a), referred to as AC that expands the complexity and diversity of the human transcriptome^{24,25}. By analyzing ribosomal RNA-depleted RNA sequencing (ribo- RNA-seq) datasets across six distinct cell lines (Supplementary Data 1), including HT29, DLD-1, LoVo, HeLa, A549 and 293FT, with the CIRCexplorer3 pipeline^{27,29}, approximately half (42% to 55%) of circRNA-producing gene loci were identified to produce multiple circRNAs (Supplementary Fig. 1a, b and Supplementary Data 2), accounting for 70% to 83% of total numbers of expressed circRNAs in each examined cell line (Fig. 1b). Although multiple (median = 3) circRNAs can be produced from each AC gene locus with current sequence depths (~50 millions of 2×100 pair-ended, Supplementary Fig. 1c), these AC circRNAs from the same gene loci were not evenly expressed. Indeed, a predominantly expressed circRNA (hereafter named pe-circRNA for simplicity) was generally observed in each AC gene, contributing to the majority (with median over 50%) of total BSJ-mapped fragments per billion mapped bases (FPBs) from the given gene locus (Fig. 1c)^{27,30}.

Detailed analyses suggested complex patterns of pe-circRNA expression among different cell lines (Supplementary Data 2). On the one hand, when compared the top 100 of pe-circRNA-expressing genes across six cell lines, most these host genes exhibited cell-type-specific expression: 153 out of 281 were unique to a single cell line, and 69 out of 281 were shared by two cell lines. In contrast, only sixteen host genes were universally expressed across all six cell lines (Supplementary Fig. 1d). On the other hand, among these universally expressed sixteen host genes (Supplementary Fig. 1d), fifteen pe-circRNAs remained the same in all six cell lines and one remained the same in five cell lines (Fig. 1d and Supplementary Data 3), indicating the

preference for AC remained consistent in constitutively expressed genes. Thus, although most top pe-circRNAs were suggested to be diversely expressed across cell lines (Fig. 1d), a small portion of universally expressed top pe-circRNAs were identified across different cell lines, indicating their potential roles in cells.

Identification of pe-*circMANIA2(2,3,4,5)* associated with CRC

In order to investigate the functions of these universally expressed pe-circRNAs, we next set to profile pe-circRNA expression in a more specific pathological context by analyzing 20 paired ribo- RNA-seq datasets of normal and colon cancer samples from patients in stage II/III colon cancer³⁰ (Supplementary Data 1). Among all 1015 parental genes producing alternatively circularized circRNAs in both normal and cancer samples, 846 out of all 1015 pe-circRNAs and 99 out of top 100 pe-circRNAs were consistently shared between paired normal and cancer samples (Supplementary Fig. 2a and Supplementary Data 2). These include most (12 out of 15) universally expressed top pe-circRNAs identified in the six examined cell lines (Fig. 1d). When comparing their expression changes in colon cancer samples versus paired normal controls, ten of the top 100 pe-circRNAs were down-regulated (Fold changes ≤ 0.667) in cancer samples, while five of them were upregulated (Fold changes ≥ 1.5) (Fig. 1e), including *circMANIA2(2,3,4,5)*, *circCAMSAPI(2,3)*, *circUBAP2(9,10,11,12)*, *circFAM120A(2,3,4,5)* and *circRSRC1(2,3)*. Interestingly, circRNAs individually produced from these five gene loci have been previously reported to be involved in cancer progression^{31–37}, however, the detailed scenario of their AC and their modes of action on cancer progression have been insufficiently dissected.

Among these five upregulated pe-circRNAs, *circMANIA2(2,3,4,5)*, which is back-spliced from *MANIA2* (*mannosidase alpha class 1A member 2*), caught our attention due to its highest expression in all examined colon cancer samples (Fig. 1e and Supplementary Fig. 2b). In the *MANIA2* gene locus, encoding one type of alpha-mannosidases for asparagine-linked (N-linked) protein glycosylation³⁸, at least six different circRNA isoforms could be identified (Fig. 1f and Supplementary Fig. 2b). These six circRNAs are *circMANIA2(2,3)*, *circMANIA2(2,3,4)*, *circMANIA2(2,3,4,5)*, *circMANIA2(2,3,4,5,6)*, *circMANIA2(2,3,4,5,6,7,8)* and *circMANIA2(7,8,9,10,11,12)*, according to the current nomenclature²⁶ that indicates their different exonic constitutions. Of note, among these isoforms, *circMANIA2(2,3,4,5)* was identified as the pe-circRNA at the *MANIA2* locus across all examined normal and cancer samples (Fig. 1f and Supplementary Fig. 2b), whose expression was not only the highest among its cognate circRNAs (Fig. 1f, bottom panel), but also among all circRNAs identified on a genome-wide scale from the 20 colon cancer samples (Fig. 1g, top panel). Despite the expression of the linear *MANIA2* transcript being also increased in colon cancer samples (Supplementary Fig. 2c), its overall level remained modest compared to all linear RNAs across examined samples (Fig. 1g, bottom panel).

Additional AC profiling in other types of cancer samples, including colon cancer (COLO), ovarian cancer (OV), lung adenocarcinoma (LUAD), prostate adenocarcinoma (PRAD), acute myeloid leukemia (AML) and breast cancer (BRCA) (Supplementary Data 1)³⁹, further demonstrated high expression of *circMANIA2(2,3,4,5)* in all examined cancer tissue samples, with modestly expressed linear cognate transcripts (Fig. 1h). Intriguingly, modestly increased expression of *circMANIA2(2,3,4,5)* was also documented in other malignancies, such as gastric cancer³¹, nasopharyngeal carcinoma⁴⁰, oral carcinoma, thyroid carcinoma, OV and LUAD⁴¹. These findings together promoted us to further explore possible biological and pathophysiologic roles of *circMANIA2(2,3,4,5)* in CRC progression.

Repression of *circMANIA2(2,3,4,5)* inhibits CRC proliferation and tumor progression

To identify the possible role of *circMANIA2(2,3,4,5)*, we first explored its subcellular localization and abundance. Single molecule fluorescence in situ hybridization (smFISH) in HT29 showed that *circMANIA2(2,3,4,5)* was mainly localized in the cytoplasm (Fig. 2a), which was further confirmed by fractionation of cytoplasmic and nuclear RNAs (Fig. 2b). Additionally, absolute quantification by RT-qPCR revealed about 92 and 23 copies of *circMANIA2(2,3,4,5)* per HT29 and DLD-1 cell, respectively (Fig. 2c), which hints its functionality in CRC. Of note, the copy number of *circMANIA2(2,3,4,5)* obtained from absolute quantification was much more than it from smFISH, due to the technical problem^{42,43}.

Next, to assess its biological function, we performed *circMANIA2(2,3,4,5)* knock down (KD) experiments in two commonly used CRC cell lines, HT29 and DLD-1, by designing shRNAs (shRNA-c1 and shRNA-c2) specifically targeting its BSJ site that spans the 5' splice site of exon5 and the 3' splice site of exon2 (Fig. 2d). As expected, shRNAs effectively reduced *circMANIA2(2,3,4,5)* expression (Fig. 2e, f) with little effect on its cognate linear *MANIA2* mRNAs (Fig. 2e) or the other two *circMANIA2* isoforms (Fig. 2f), in examined HT29 and DLD-1 cells. Importantly, *circMANIA2(2,3,4,5)* KD led to significant inhibition of cell proliferation by MTT assays (Fig. 2g), which was also confirmed by colony formation assays (Fig. 2h). These data suggested that *circMANIA2(2,3,4,5)* might play a role in regulating cell proliferation.

Finally, we constructed xenograft tumor models to examine the effect of *circMANIA2(2,3,4,5)* in vivo. After subcutaneously injecting *circMANIA2(2,3,4,5)*-KD HT29 and DLD-1 cells into nude mice, we monitored the tumor growth at different time points from day 7. We found that *circMANIA2(2,3,4,5)* KD clearly inhibited xenograft tumor growth of HT29 and DLD-1 cells (Fig. 2i) with significantly reduced tumor size (Fig. 2j) and weight (Fig. 2k). We also developed orthotopic tumor models by inoculating *circMANIA2(2,3,4,5)*-KD HT29 and DLD-1 cells into cecum termini of NOD scid gamma (NSG) mice to further simulate CRC progression⁴⁴. Reduced tumor size (Fig. 2l) and weight (Fig. 2m) were also observed with *circMANIA2(2,3,4,5)* KD HT29 and DLD-1 cells compared to the scramble control, confirming the role of *circMANIA2(2,3,4,5)* in CRC development.

How could *circMANIA2(2,3,4,5)* regulate cell proliferation? As reported, a few cytoplasmic circRNAs could produce functional peptides during tumorigenesis⁴⁵, we evaluated whether *circMANIA2(2,3,4,5)* could encode peptide(s). Interestingly, despite of containing two predicted open reading frames with TransCirc⁴⁶ (Supplementary Fig. 3a), no obvious FLAG-tagged protein signal was detected with the in-frame insertion of a FLAG-coding sequence upstream of the stop codon (Supplementary Fig. 3b). These analyses indicated that the observed function of *circMANIA2(2,3,4,5)* on cell proliferation and CRC development was likely independent on its coding potential, but rather its noncoding RNA feature.

The association of IGF2BP2 protein with *circMANIA2(2,3,4,5)*

To gain insights into the mechanism of how *circMANIA2(2,3,4,5)* regulate cell proliferation, we set to identify *circMANIA2(2,3,4,5)*-

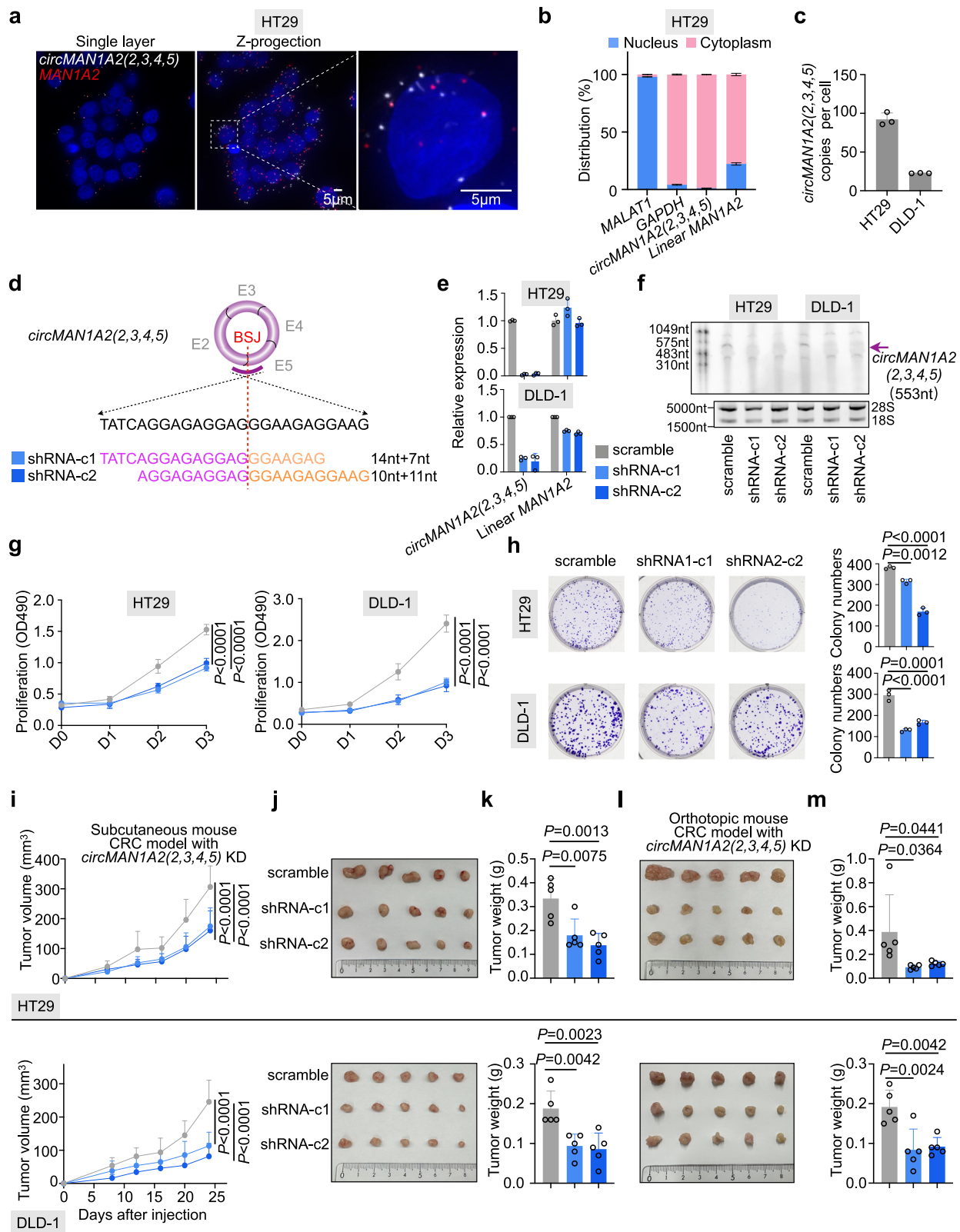
associated proteins. With an optimized in vitro transcription and circularization approach (IVC, "Methods")^{47,48}, we synthesized biotin-labeled *ivcMANIA2(2,3,4,5)* that mimics the endogenous *circMANIA2(2,3,4,5)* for RNA pull-down assays (Fig. 3a), and the biotin-labeled *EGFP* RNA was used as a control. By comparing enriched proteins with biotin-*ivcMANIA2(2,3,4,5)*, but not biotin-*EGFP* (unique peptide ≥ 1 , fold change > 2 and P value < 0.05 , "Methods"), a total of 36 *ivcMANIA2(2,3,4,5)*-enriched proteins were identified (Supplemental Data 4). Gene ontology (GO) analysis of these enriched proteins revealed their functions were mainly associated with RNA or protein-related biological processes (Supplementary Table 1), including IGF2BP2 (Fig. 3b), with reported role in modulating mRNA stability^{49,50}. The association of *ivcMANIA2(2,3,4,5)* with endogenous IGF2BP2 from HT29 cell lysates (Fig. 3c, top panel) or purified IGF2BP2 from *Escherichia coli* (Fig. 3c, bottom panel) was further confirmed by Western Blot (WB). Meanwhile, electrophoretic mobility shift assays (EMSA) further supported the interaction between *ivcMANIA2(2,3,4,5)* with IGF2BP2, but not EGFP (Fig. 3d). Additionally, native ribonucleo-protein immunoprecipitation (RIP) assays also revealed IGF2BP2 was specifically associated with endogenous *circMANIA2(2,3,4,5)*, linear *MANIA2* mRNA, but not negative controls (*GAPDH* or *U6*) (Fig. 3e).

Of note, all the in-cell pull-down, in vitro pull-down, EMSA, and RIP assays revealed that linear *MANIA2(2,3,4,5)* could also associate with IGF2BP2 (Fig. 3c–e), due to the full sequence overlap between *ivcMANIA2(2,3,4,5)* and linear *MANIA2(2,3,4,5)* except the BSJ site. In line with this, four anti-IGF2BP2-enriched eCLIP signals (c1, c2, c3 and c4) retrieved from the published IGF2BP2 eCLIP dataset (GEO, GSE91445) were shown at exons 2 to 5 of the *MANIA2* gene (Fig. 3f). In order to investigate the specific association site(s) of IGF2BP2 on *circMANIA2(2,3,4,5)*, we designed four LNAs, individually pairing to each of the four enriched IGF2BP2 eCLIP signals, nucleotides 552–553 of exon5 and nucleotides 1–21 of exon2 (LNA-c1), 183–208 of exon2 (LNA-c2), 289–312 of exon3 (LNA-c3) or 353–375 of exon4 (LNA-c4) on *MANIA2* (GENCODE transcript: ENST00000356554.7), for the LNA blocked-in vitro RNA pull-down and WB analyses. Of note, the LNA-c1 exactly spanned the BSJ site. Briefly, the biotin-labeled *EGFP*, linear *MANIA2(2,3,4,5)*, or *ivcMANIA2(2,3,4,5)* were first annealed with individual LNAs to block their binding sites, and then incubated with IGF2BP2 to evaluate the extent to which IGF2BP2 still bound to these different RNAs by in vitro RNA pull-down analyses. Subsequent WB showed LNA-c1, LNA-c2 and LNA-c3, but not LNA-c4, significantly impaired the interaction of *ivcMANIA2(2,3,4,5)* with IGF2BP2 (Fig. 3g), suggesting the requirement of nucleotides 552–21, 183–208, and 289–312 in *circMANIA2(2,3,4,5)* for its specific association with IGF2BP2.

Then, how could the direct interaction between *circMANIA2(2,3,4,5)* and IGF2BP2 regulate cell proliferation and cancer progression? As IGF2BP2 was shown to modulate mRNA stability^{49,50}, we then questioned whether the association of IGF2BP2 with *circMANIA2(2,3,4,5)* could also stabilize *circMANIA2(2,3,4,5)* expression. Interestingly, *IGF2BP2* KD (Fig. 3h, left panel) showed little effect on *circMANIA2(2,3,4,5)* expression (Fig. 3h, right panel) in DLD-1 cells, and *circMANIA2(2,3,4,5)* KD (Fig. 2e, bottom panel) exhibited little effect on *IGF2BP2* expression (Fig. 3i). These results suggest that the association between IGF2BP2 and *circMANIA2(2,3,4,5)* does not regulate *circMANIA2(2,3,4,5)* stability, but rather might play other roles in gene expression regulation.

CENPB is the major downregulated gene upon loss of *circMANIA2(2,3,4,5)*

To identify altered genes along with *circMANIA2(2,3,4,5)* KD, we first performed ribo- RNA-seq analyses in multiple *circMANIA2(2,3,4,5)* KD cell lines, including HT29, DLD-1, HeLa, A549 and 293FT (Supplemental Data 5). From ribo- RNA-seq datasets, differentially expressed linear RNAs and the expression of circRNAs could be individually determined with edgeR⁵¹ or CIRCexplorer3 (Fig. 4a)^{27,29}. As expected,



circMAN1A2(2,3,4,5) was efficiently depleted in all examined cell lines, while its cognate linear RNA expression (Fig. 4b) remained unchanged, demonstrating the specificity of *circMAN1A2(2,3,4,5)* KD.

Next, the analysis of differentially expressed genes (DEGs) was obtained by comparing their expression levels to those in the scramble group (Supplementary Fig. 4a, b). Interestingly, only three down-regulated DEGs, including *CENPB*, *BCL2L2-PABPN1* and *PABPN1*, were

identified upon *circMAN1A2(2,3,4,5)* KD in all five examined cell lines, without upregulated genes (Fig. 4c and Supplementary Fig. 4b). Among all three downregulated genes, *CENPB* expression exhibited the most significant fold change with a high background expression level (Fig. 4c and Supplementary Fig. 4c). *CENPB* is essential for mammalian centromeric function by orchestrating three fundamental processes: (1) facilitating CENPA deposition and stabilization at

Fig. 2 | Repression of *circMANIA2(2,3,4,5)* inhibits colorectal cancer cell proliferation and tumor progression. **a, b** *CircMANIA2(2,3,4,5)* was mainly localized in the cytoplasm of HT29 cells, as revealed by smFISH staining of *circMANIA2(2,3,4,5)* (white), *MANIA2* (red) and nuclei (blue) (**a**), and fractionation of the cytoplasmic and nuclear RNA assay (**b**; $n = 3$ independent experiments) with *GAPDH* and *MALAT1* as cytoplasmic and nuclear RNA markers. **c** Copy numbers of *circMANIA2(2,3,4,5)* in HT29 and DLD-1. **d** Designed shRNA-c1 and shRNA-c2 specifically targeting the BSJ site of *circMANIA2(2,3,4,5)*, both spanning the 5' splice site of exon5 and the 3' splice site of exon2. nt, nucleotide. **e, f** KD efficiency of *circMANIA2(2,3,4,5)* in HT29 and DLD-1 cells, as detected by RT-qPCR and normalized to *ACTB* (**e**) and Northern Blot (NB) (**f**) with violet arrow represents *circMANIA2(2,3,4,5)*. **g, h** KD of *circMANIA2(2,3,4,5)* inhibited cell proliferation in HT29 and DLD-1 cells, as revealed by MTT cell proliferation assay (**g**; $n = 5$ wells of cells examined over 3 independent experiments) and colony formation assay (**h**) with representative images of cell colonies (left panel) and statistics of colony numbers (right panel). **i–k** Tumor growth curves from nude mice injected subcutaneously

with scramble and *circMANIA2(2,3,4,5)*-KD HT29 (top panel) and DLD-1 cells (bottom panel) were shown in (**i**); the images of tumors were shown in (**j**); statistics of tumor weight were shown in (**k**). Tumor size was measured every 4 days for 24 days and calculated as width² × length × 0.5. $n = 5$ biologically independent samples. **l, m** The image of tumors from NSG mice injected cecum with scramble and *circMANIA2(2,3,4,5)*-KD HT29 (top panel) and DLD-1 cells (bottom panel) were shown in (**l**); statistics of tumor weight were shown in (**m**). $n = 5$ biologically independent samples. RNA levels were detected by RT-qPCR (**b**). Images are representative of three independent experiments (**a, f, h**). Data are presented as mean ± s.d. (**b, c, e, g–i, k, m**), with biologically individual data points shown (**c, e, h, k, m**). P values were determined by ordinary two-way ANOVA with Dunnett's post-hoc comparisons versus scramble control at each row factor level (adjusted P values) (**g, i**) and ordinary one-way ANOVA test with Dunnett's post-hoc comparisons versus scramble control (FDR-adjusted P values) (**h, k, m**). Source data are provided as a Source Data file.

centromeric chromatin⁵²; (2) recruiting CENPC to establish the constitutive centromere-associated network core complex⁵³; (3) preserving epigenetic memory of centromere identity across cell cycles⁵⁴. *CENPB* depletion induces premature centromere separation, merotelic kinetochore attachments and chromosome mis-segregation, resulting in aneuploidy, a hallmark causally linked to oncogenesis^{55,56}. The downregulated *CENPB* expression upon *circMANIA2(2,3,4,5)* KD was confirmed by RT-qPCR and WB in both HT29 (Fig. 4d) and DLD-1 cells (Fig. 4e).

To exclude possible off-target effects by shRNA KD, we also utilized the RfxCas13d system, which can effectively discriminate circRNA from linear RNA^{33,57}, to KD *circMANIA2(2,3,4,5)* (Fig. 4f). As expected, successful KD of *circMANIA2(2,3,4,5)* (but not linear *MANIA2* RNAs) by RfxCas13d-BSJ-sgRNAs (Fig. 4g), resulted in decreased expression of *CENPB* at both RNA (Fig. 4h, left panel) and protein (Fig. 4h, right panel) levels in DLD-1 cells, confirming the notion that *circMANIA2(2,3,4,5)* can modulate *CENPB* gene expression.

IGF2BP2 interacts with *CENPB* mRNA and regulates its expression

Our results demonstrated that *circMANIA2(2,3,4,5)* could associate with IGF2BP2 (Fig. 3). Giving the cytoplasmic localization of *CENPB* mRNA (Fig. 5a), we were surprised to find that enriched IGF2BP2 signals were also detected in the *CENPB* mRNA in the same IGF2BP2 eCLIP datasets (GEO, GSE91445) (Fig. 5b). Further in-cell and in vitro RNA pull-down assays (Fig. 5c) showed that IGF2BP2 preferentially interacted with *CENPB*-3' untranslated region (*CENPB*-3'UTR) than with the *CENPB* coding sequence (*CENPB*-CDS) (Fig. 5d). This notion was further confirmed by EMSA assays, which detected a more pronounced shift at a lower RNA:IGF2BP2 molar ratio in the *CENPB*-3'UTR (1:10) compared to the *CENPB*-CDS (1:40) (Fig. 5e). Meanwhile, RIP assays with anti-IGF2BP2 antibody further validated the endogenous interaction between IGF2BP2 and *CENPB* mRNA (Fig. 5f). With designed LNAs (LNA-b1, b2 and b3) pairing to the IGF2BP2 enriched signals on *CENPB*-3'UTR (GENCODE transcript: ENST00000379751.5) region (Fig. 5b), similar LNA-blocked RNA pull-down assays were performed using biotin-labeled *EGFP* and the *CENPB*-3'UTR. These showed that LNA-b2 (nucleotides 2575–2615), but not LNA-b1 (nucleotides 2232–2280) or LNA-b3 (nucleotides 2759–2805), could significantly block the association between *CENPB*-3'UTR and IGF2BP2 (Fig. 5g), suggesting their specific interaction relying on the nucleotides 2575–2615 of *CENPB*-3'UTR.

Given the specific interaction between IGF2BP2 and *CENPB* mRNA, we next examined the effect of IGF2BP2 on the expression of *CENPB* mRNA. As shown in Fig. 5h, *IGF2BP2* KD led to a significant reduction in *CENPB* mRNA, and a modest effect on *CENPB* protein. In addition, we also treated cells with small-molecule inhibitor (CWII-2) that competitively binds to IGF2BP2⁵⁰, resulting in a similar downregulation of

CENPB mRNA and protein level (Fig. 5i). Furthermore, to block the interaction between IGF2BP2 and *CENPB* mRNA, we transfected DLD-1 cells with LNA-b2, which resulted in a significant reduction of *CENPB* mRNA levels (Fig. 5j). These findings together suggested that IGF2BP2 binds to the 3'UTR of *CENPB* mRNA and regulates its expression.

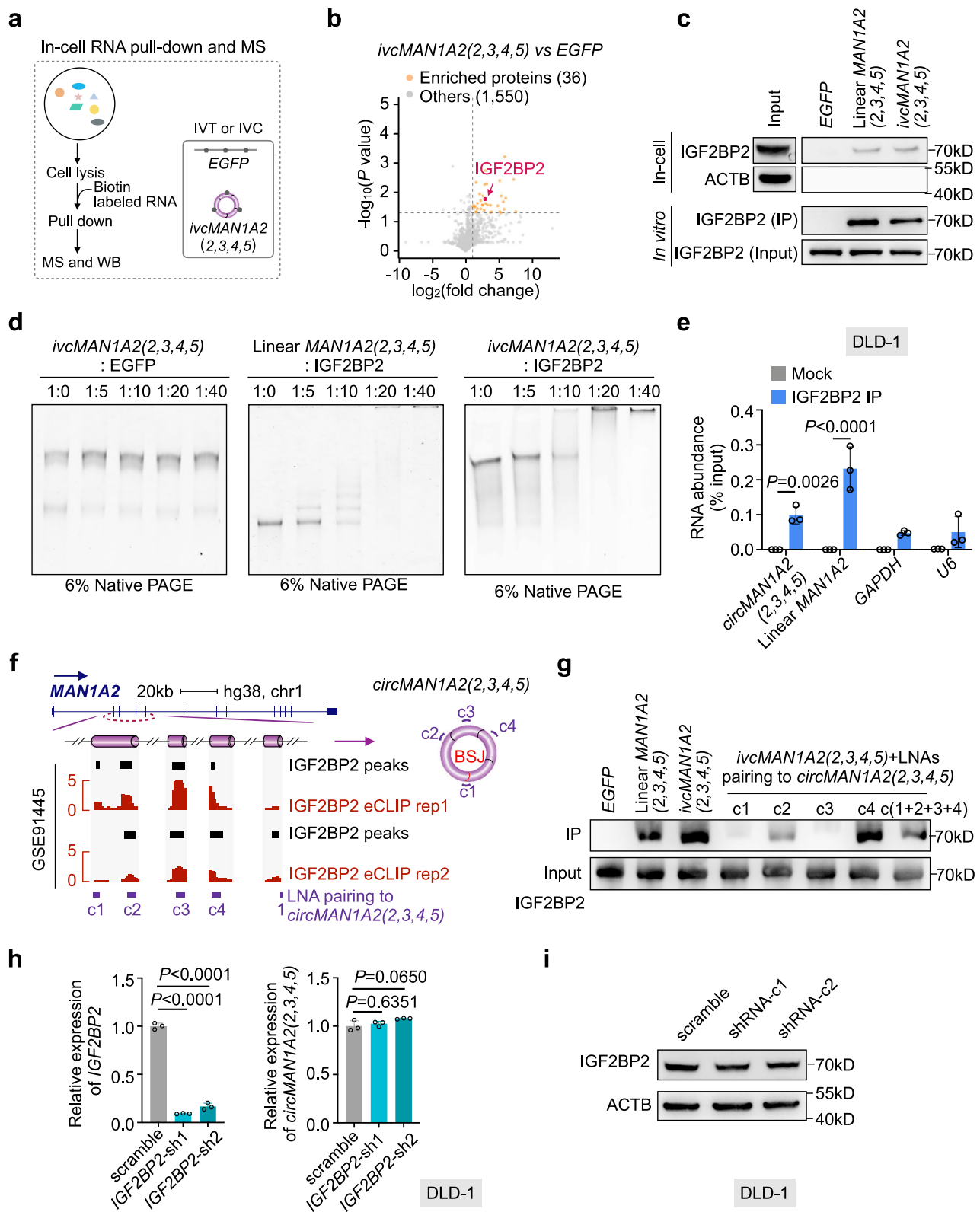
Direct RNA-RNA interaction between *circMANIA2(2,3,4,5)* and *CENPB* mRNA

In addition to IGF2BP2, *circMANIA2(2,3,4,5)* KD also repressed *CENPB* mRNA expression in all examined cell lines. Absolute quantification by RT-qPCR revealed about 19 and 13 copies of *CENPB* mRNA per HT29 and DLD-1 cell, respectively (Supplementary Fig. 5a), revealing similar stoichiometric ratios with *circMANIA2(2,3,4,5)* (Fig. 2c). Given that IGF2BP2 regulates *CENPB* expression through direct binding, we thus asked whether *circMANIA2(2,3,4,5)* might also directly interact with *CENPB* mRNA.

To test this idea, we performed RNA pull-down in cells treated with 4'-aminome-thyltrioxsalen (AMT, a psoralen derivative), a cross-linker that stabilizes interactions between nucleic acids⁵⁸. With specific biotin-labeled antisense probes that individually targeting *EGFP* mRNA (as a negative control), linear *MANIA2* or *circMANIA2(2,3,4,5)*, these individual RNAs and their interacting RNAs could be precipitated and then detected by RT-qPCR (Fig. 6a). As shown in Fig. 6b, the biotin-labeled antisense probes targeting *circMANIA2(2,3,4,5)* enriched much more *CENPB* mRNAs than those targeting *EGFP* and linear *MANIA2*. As another control, the enrichment of *GAPDH* mRNAs showed no significant difference among all groups, indicating the specific interaction between *circMANIA2(2,3,4,5)* and *CENPB* mRNA (Fig. 6b).

The interaction between *circMANIA2(2,3,4,5)* and *CENPB* mRNA was also confirmed by additional RNA pull-down assays. Briefly, we prepared biotin-labeled *EGFP*, linear *MANIA2(2,3,4,5)* and *ivcMANIA2(2,3,4,5)*, which were individually incubated with *CENPB*-CDS or *CENPB*-3'UTR, followed by examining to what degree that *CENPB* RNAs directly interact with *ivcMANIA2(2,3,4,5)*, compared to controls (Fig. 6c). As shown in Fig. 6d, the biotin-labeled *ivcMANIA2(2,3,4,5)* directly interacted with *CENPB*-3'UTR, but not *CENPB*-CDS; while the biotin-labeled linear *MANIA2(2,3,4,5)* showed much weaker interaction with *CENPB*-3'UTR and no interaction with *CENPB*-CDS. As the primary sequence of linear *MANIA2(2,3,4,5)* fully overlaps that of *ivcMANIA2(2,3,4,5)* except the characteristic BSJ sequence, the specific and strong interaction between *ivcMANIA2(2,3,4,5)* and *CENPB*-3'UTR suggested that their association could be dependent on the BSJ sequence of *circMANIA2(2,3,4,5)*.

To further identify the specific binding sequences between *circMANIA2(2,3,4,5)* and *CENPB*-3'UTR, we used the IntaRNA algorithm⁵⁹ to predict corresponding sequences for their direct interaction. Strikingly, a thirteen-nucleotide sequence (nucleotides 550–553 of exon5 and 1–9 of exon2) spanning the BSJ site of *circMANIA2(2,3,4,5)*



was exactly complementary to a sequence within the *CENPB*-3'UTR (nucleotides 2268–2280) (Fig. 6e, color highlight). In addition, another nine-nucleotide sequence in the exon2 (nucleotides 16–24) of *circMANIA2(2,3,4,5)* was also predicted to base pair with the *CENPB*-3'UTR (nucleotides 2258–2266).

To verify the predicted binding sites, we designed two specific LNAs, individually pairing to the predicted sequences in *circMANIA2(2,3,4,5)* BSJ (LNA-BSJ) or exon2 (LNA-Ex2) (Fig. 6e) for the LNA

blocked in vitro RNA pull-down assays. Of note, similar procedures were performed as shown in Fig. 6c except that the biotin-labeled *EGFP*, linear *MANIA2(2,3,4,5)*, and *ivcMANIA2(2,3,4,5)* were pre-annealed with paired LNAs before incubating with *CENPB*-3'UTR. As shown in Fig. 6f, blocking with LNA-BSJ, but not LNA-Ex2, significantly reduced the enrichment of *CENPB*-3'UTR by *ivcMANIA2(2,3,4,5)*. Moreover, the third LNA (LNA-UTR) against the nucleotides 2258–2280 of *CENPB*-3'UTR also significantly blocked the interaction between *CENPB*-3'UTR

Fig. 3 | The association of IGF2BP2 protein with *circMANIA2(2,3,4,5)*. **a** Schematic of in-cell RNA pull-down assay using *EGFP* and *ivcMANIA2(2,3,4,5)*, followed by mass spectrum (MS) analysis ($n = 2$ independent experiments). **b** Volcano plot of enriched protein candidates via in-cell *ivcMANIA2(2,3,4,5)* RNA pull-down assay followed by MS ($n = 2$ independent experiments). *EGFP* RNA was a negative control. IGF2BP2 is highlighted in red. **c** *ivcMANIA2(2,3,4,5)* and linear *MANIA2(2,3,4,5)* interacted with IGF2BP2, as revealed by in-cell (top panel) and in vitro (bottom panel) RNA pull-down assay followed by Western Blot (WB). **d** IGF2BP2 interacted with *ivcMANIA2(2,3,4,5)* and linear *MANIA2(2,3,4,5)*, as revealed by EMSA. *EGFP* protein was a negative control. **e** IGF2BP2 enriched more endogenous *circMANIA2(2,3,4,5)* and linear *MANIA2*, as detected by native RIP assay. IgG was performed as a negative control; *GAPDH* mRNA and *U6* RNA were detected as negative controls. **f** Identified IGF2BP2-binding sequence in *circMANIA2(2,3,4,5)*. Top, genomics locus and diagram of linear *MANIA2* and *circMANIA2(2,3,4,5)* (shown as cylinders in magenta). Bottom, IGF2BP2 binding peaks

and wiggle-tracks from eCLIP-seq data in K562 cells (GEO, GSE91445) revealed that IGF2BP2 proteins could binding at the *circMANIA2(2,3,4,5)*. LNAs pairing to *circMANIA2(2,3,4,5)* are shown as violet lines. **g** LNA-blocked in vitro RNA pull-down assay revealed the specific binding sites of IGF2BP2 on *circMANIA2(2,3,4,5)*. **h** KD of *IGF2BP2* showed a negligible effect on *circMANIA2(2,3,4,5)* expression. Left panel: KD efficiency of *IGF2BP2* in DLD-1 cells. Right panel: *circMANIA2(2,3,4,5)* expression level. **i** KD of *circMANIA2(2,3,4,5)* barely affected IGF2BP2 expression in DLD-1 cells. Images are representative of three independent experiments (**c**, **d**, **g**, **i**). RNA levels were detected by RT-qPCR (**e**, **h**), normalized to *ACTB* (**h**) and presented as mean \pm s.d., with biologically individual data points shown (**e**, **h**). *P* values were determined by two-tailed Welch's *t*-tests without correction for multiple comparisons (**b**), ordinary two-way ANOVA with Dunnett's post-hoc comparisons versus scramble control at each row factor level (adjusted *P* values) (**e**) and ordinary one-way ANOVA test with Dunnett's post-hoc comparisons versus scramble control (FDR-adjusted *P* values) (**h**). Source data are provided as a Source Data file.

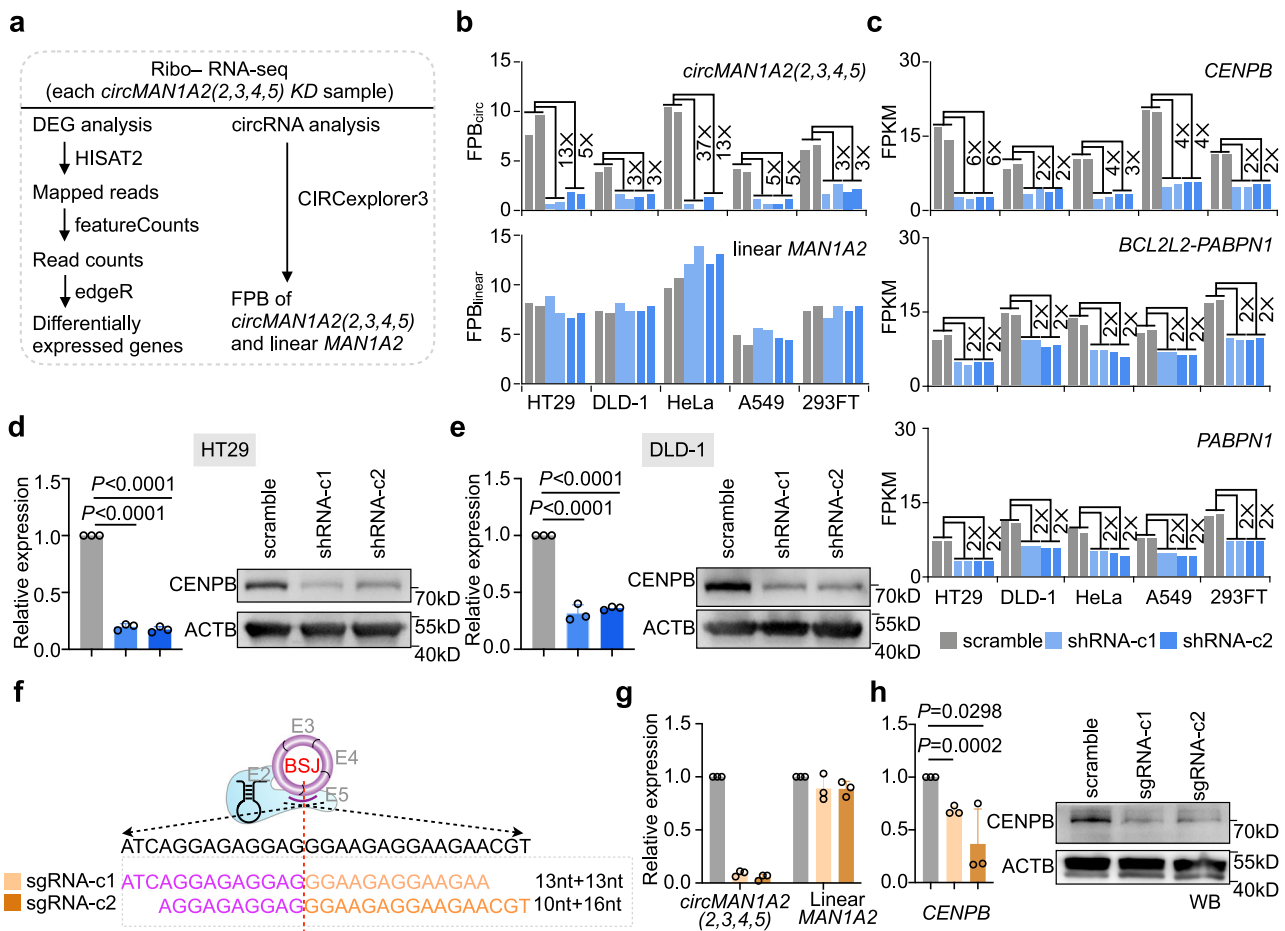


Fig. 4 | *CENPB* is the major downregulated gene upon loss of *circMANIA2(2,3,4,5)*. **a** Computational pipeline to identify differentially expressed genes and circRNAs after KD of *circMANIA2(2,3,4,5)*. **b** KD of *circMANIA2(2,3,4,5)* reduced *circMANIA2(2,3,4,5)* expression but not linear *MANIA2*. FPB_{circ} of *circMANIA2(2,3,4,5)* (top panel) and FPB_{linear} of linear *MANIA2* (bottom panel) were shown in corresponding HT29, DLD-1, HeLa, A549, and 293FT cell lines with *circMANIA2(2,3,4,5)* KD. **c** KD of *circMANIA2(2,3,4,5)* reduced *CENPB*, *BCL2L2-PABPN1* and *PABPN1* mRNA expression. FPKM of each mRNA was shown in corresponding HT29, DLD-1, HeLa, A549, and 293FT cell lines with *circMANIA2(2,3,4,5)* KD. **d**, **e** KD of *circMANIA2(2,3,4,5)* led to downregulated *CENPB* expression in HT29 (**d**) and DLD-1 cells (**e**), as shown by RT-qPCR (left panels) and WB (right panels). **f** Designed

sgRNA-c1 and sgRNA-c2 specifically targeting the BSJ site of *circMANIA2(2,3,4,5)* for RfxCas13d system. **g** KD efficiency of *circMANIA2(2,3,4,5)* by RfxCas13d in DLD-1 cells. **h** KD of *circMANIA2(2,3,4,5)* by RfxCas13d led to downregulated *CENPB* expression in DLD-1 cells detected by RT-qPCR (left panel) and WB (right panel). Images are representative of three independent experiments (**d**, **e**, **h**). RNA levels were detected by RT-qPCR, normalized to *ACTB* and presented as mean \pm s.d., with biologically individual data points shown (**d**, **e**, **g**, **h**). *P* values were determined by ordinary one-way ANOVA test with Dunnett's post-hoc comparisons versus scramble control (FDR-adjusted *P* values) (**d**, **e**) and unpaired two-tailed Student's *t*-test (**h**). Source data are provided as a Source Data file.

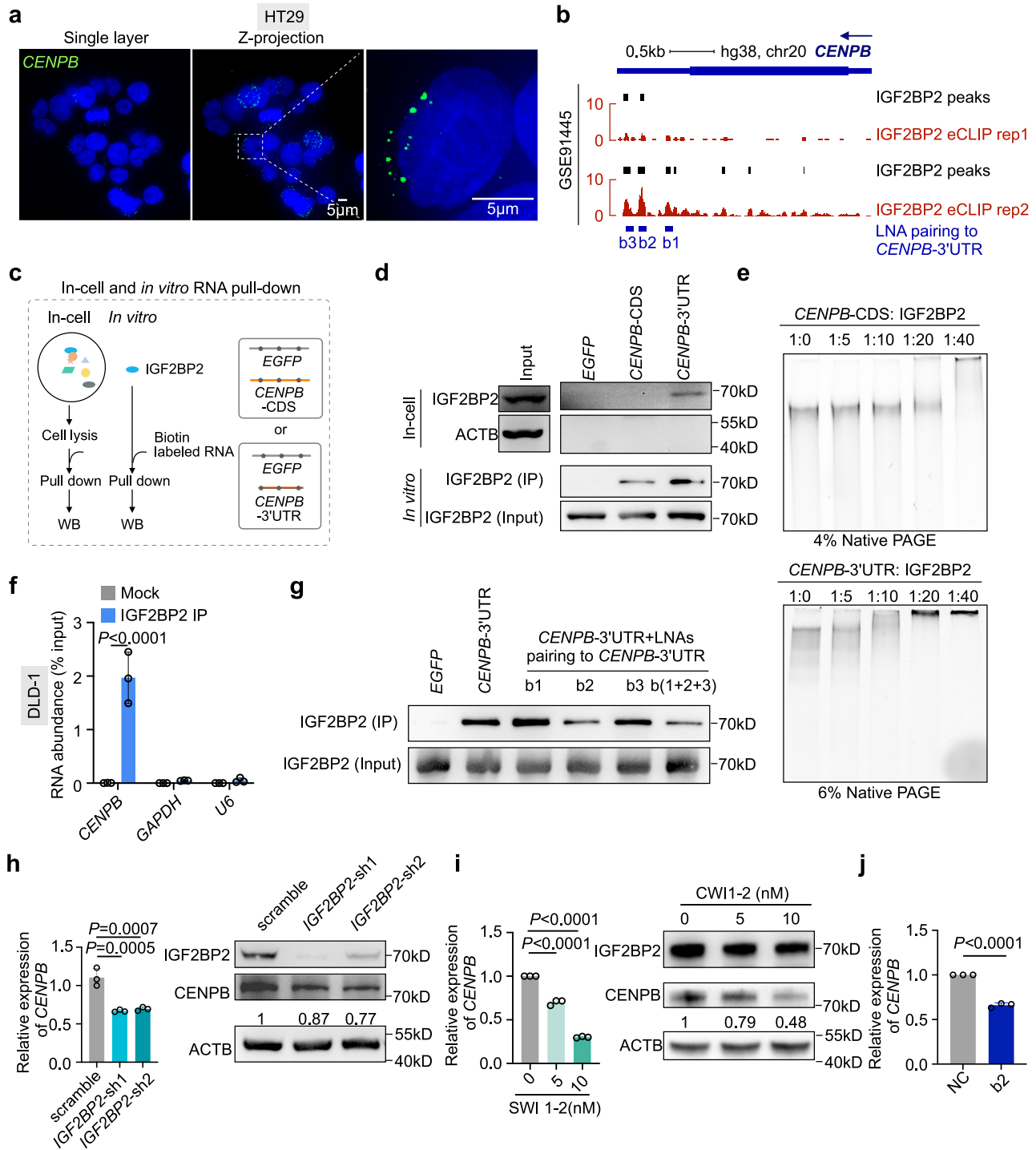
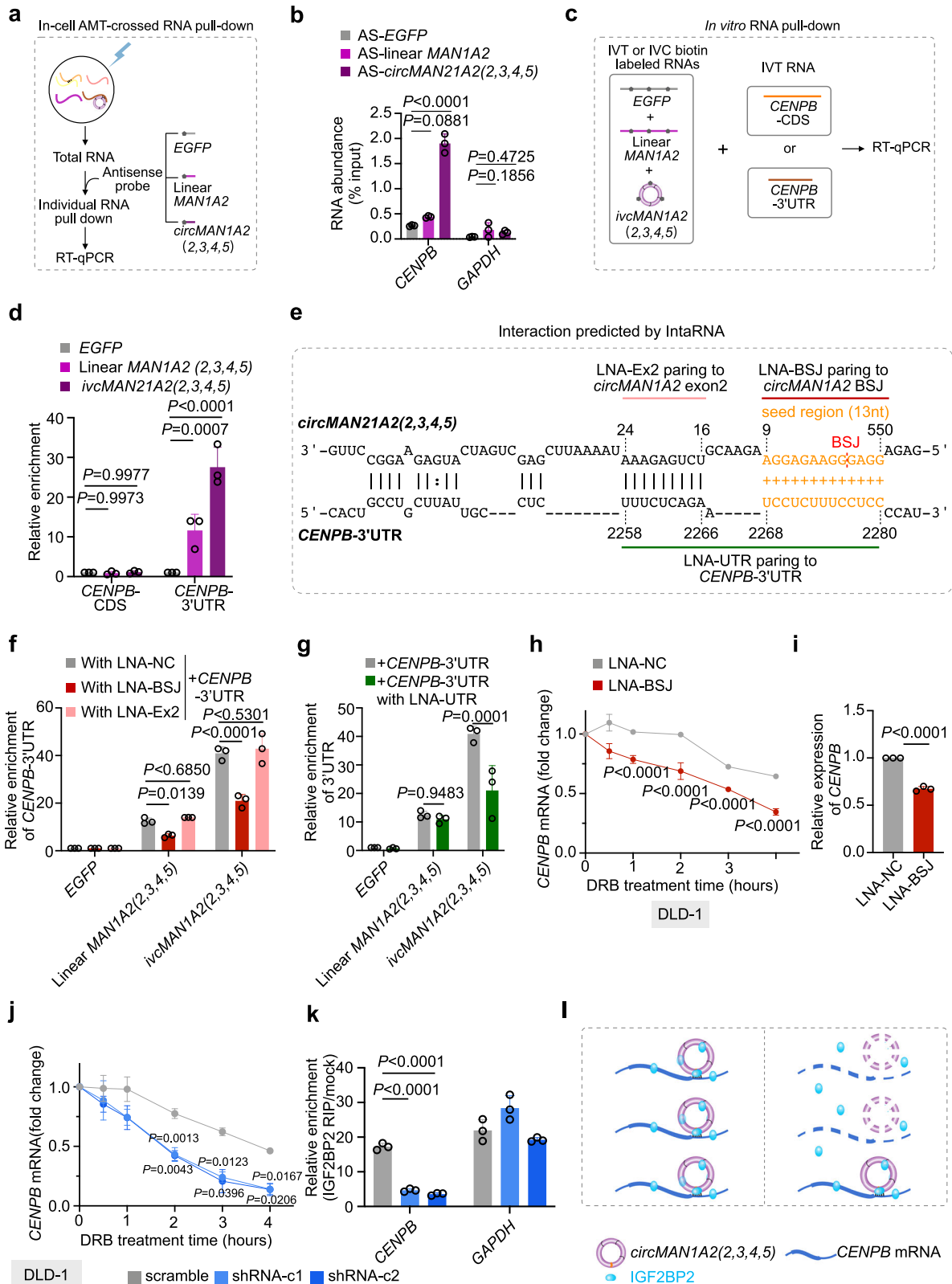


Fig. 5 | IGF2BP2 interacts with *CENPB* mRNA and regulates its expression.

a Localization of *CENPB* mRNA in HT29 cells, as revealed by smFISH staining of *CENPB* (green) and nuclei (blue). **b** Identified IGF2BP2-binding sequence in the 3' UTR and CDS regions of *CENPB* mRNA. Top, genomics locus and diagram of *CENPB* mRNA. Bottom, IGF2BP2 binding peaks and wiggle-tracks of data from eCLIP-seq in K562 cells. LNAs pairing to *CENPB*-3'UTR are shown as navy lines. **c** Schematic of in-cell and in vitro RNA pull-down assay. **d, e** *CENPB*-3'UTR, but not *CENPB*-CDS, preferentially to bind to IGF2BP2, as revealed by in-cell (top panel) and in vitro (bottom panel) RNA pull-down assay (**d**) and EMSA assay (**e**). **f** IGF2BP2 enriched more endogenous *CENPB* mRNA, as detected by native RIP assay. IgG was performed as a negative control; *GAPDH* mRNA and *U6* RNA were detected as negative controls. **g** LNA-blocked RNA pull-down assay revealed the specific binding sites of

IGF2BP2 on *CENPB*-3'UTR. **h, i** KD of IGF2BP2 (**h**) and CWI1-2 (5 nM and 10 nM) treatment (**i**) reduced *CENPB* expression in DLD-1 cells, as shown by RT-qPCR (left panel) and WB (right panel). **j** LNA-b2 reduced *CENPB* expression in DLD-1 cells. Images are representative of three independent experiments (**a, d, e, g-i**). RNA levels were detected by RT-qPCR (**f, h-j**), normalized to *ACTB* (**h-j**) and are presented as mean \pm s.d., with biologically individual data points shown (**f, h-j**). *P* values were determined by ordinary two-way ANOVA with Dunnett's post-hoc comparisons versus scramble control at each row factor level (adjusted *P* values) (**f**), ordinary one-way ANOVA test with Dunnett's post-hoc comparisons versus scramble control (FDR-adjusted *P* values) (**h, i**), and unpaired two-tailed Student's *t*-test (**j**). Source data are provided as a Source Data file.



and *ivcMANIA2(2,3,4,5)*, but not IVT linear *MANIA2(2,3,4,5)* (Fig. 6g). Additionally, dual LNAs blocking using LNA-BSJ and LNA-UTR significantly improved the inhibition efficiency compared to single LNA (Supplementary Fig. 5b). These results together suggested a direct interaction between *circMANIA2(2,3,4,5)* and *CENPB* mRNA, specifically through the BSJ sequence of *circMANIA2(2,3,4,5)* and the *CENPB*-3'UTR region (nucleotides 2268–2280).

The direct interaction between *circMANIA2(2,3,4,5)* and *CENPB* mRNA enhances the IGF2BP2-mediated *CENPB* mRNA stability
 What is the consequence of the direct interaction between *circMANIA2(2,3,4,5)* and *CENPB* mRNA? We found IGF2BP2 to be associated with both *circMANIA2(2,3,4,5)* (Fig. 3c–e) and *CENPB* mRNA (Fig. 5d–f), and IGF2BP2 inhibition alone repressed the expression of *CENPB* mRNA (Fig. 5h, i), but not *circMANIA2(2,3,4,5)* (Fig. 3h). We speculated

Fig. 6 | The direct interaction between *circMANIA2(2,3,4,5)* and *CENPB* mRNA enhances the IGF2BP2-mediated *CENPB* mRNA stability. **a** Schematic of in-cell AMT-crossed RNA pull-down assay. **b** *CircMANIA2(2,3,4,5)* interacted with *CENPB* mRNA in vivo, as revealed by in-cell AMT-crossed RNA pull-down assay. *GAPDH* mRNA is a negative control. **c** Schematic of in vitro RNA pull-down assay. **d** *lucMANIA2(2,3,4,5)* interacted with *CENPB*-3'UTR in vitro, as revealed by in vitro RNA pull-down assay. **e** Prediction of RNA interaction sequences between *CENPB* mRNA and *circMANIA2(2,3,4,5)* by IntaRNA. The yellow highlight indicates seed region of interacted sequence, which exactly covers the BJS site of *circMANIA2(2,3,4,5)*. The pink and red lines indicate LNA pairing to exon2 and BJS sequence of *circMANIA2(2,3,4,5)*, respectively. The green line indicates LNA pairing to 3'UTR of *CENPB* mRNA. **f** LNA-blocked RNA pull-down assay revealed the specific binding sites of *CENPB*-3'UTR on *circMANIA2(2,3,4,5)*. **g** LNA-blocked RNA pull-down assay revealed the specific binding sites of *circMANIA2(2,3,4,5)* on *CENPB*-3'UTR. **h** LNA-BSJ reduced *CENPB* mRNA stability in DLD-1 cells ($n = 3$ independent

experiments). LNA-NC and LNA-BSJ were transfected into DLD-1 for 48 h and then were treated with DRB (100 μ M) for 0, 0.5, 1, 2, 3, and 4 h followed by RNA isolation and RT-qPCR. **i** LNA-BSJ reduced *CENPB* mRNA level in DLD-1 cells. **j** KD of *circMANIA2(2,3,4,5)* reduced *CENPB* mRNA stability in DLD-1 cells ($n = 3$ independent experiments). **k** KD of *circMANIA2(2,3,4,5)* reduced the association of IGF2BP2 on *CENPB* mRNA in DLD-1 cells, as revealed by native RIP assay. **l** A proposed model of *circMANIA2(2,3,4,5)*-IGF2BP2-*CENPB*-3'UTR interaction. Through directly RNA-RNA interaction, *circMANIA2(2,3,4,5)* enhanced the association of IGF2BP2 on *CENPB* mRNA, which impacting its mRNA stability and expression. RNA levels were detected by RT-qPCR (**b**, **d**, **f-k**), normalized to *ACTB* (**i**) and presented as mean \pm s.d. (**b**, **d**, **f-k**), with biologically individual data points shown (**b**, **d**, **f**, **g**, **i**, **k**). *P* values were determined by ordinary two-way ANOVA with Dunnett's post-hoc comparisons versus scramble control at each row factor level (adjusted *P* values) (**b**, **d**, **f-h**, **j**, **k**) and unpaired two-tailed Student's *t*-test (**i**). Source data are provided as a Source Data file.

that the direct binding of *circMANIA2(2,3,4,5)* with *CENPB* mRNA might affect its stability through IGF2BP2.

To further investigate this hypothesis, we measured the degradation rate of *CENPB* mRNA after transfecting LNA-BSJ into DLD-1 cells to block the RNA-RNA interaction. With the treatment of 1- β -D-ribofuranoside (DRB), which inhibits Pol II transcription, we found that LNA-BSJ markedly accelerated the degradation rate of *CENPB* mRNA (Fig. 6h) and decreased its mRNA level (Fig. 6i). Additionally, we also observed the decreased *CENPB* mRNA stability in *circMANIA2(2,3,4,5)* KD cell lines (Fig. 6j). These results suggested the direct interaction between *circMANIA2(2,3,4,5)* and *CENPB* mRNA regulated *CENPB* mRNA stability.

Given the known role of IGF2BP2 in mRNA stability^{49,50}, we speculated that the observed phenomenon might be due to changes of IGF2BP2 binding. Indeed, our results showed that *circMANIA2(2,3,4,5)* KD significantly inhibited IGF2BP2 binding to *CENPB* mRNA, but not to the control, *GAPDH* mRNA (Fig. 6k). Furthermore, when LNA-c(1+2+3) blocked the binding of IGF2BP2 on *circMANIA2(2,3,4,5)* (Supplementary Fig. 5c), both mRNA stability and expression level of *CENPB* decreased (Supplementary Fig. 5d, e). These results together suggested that through direct RNA-RNA interaction, *circMANIA2(2,3,4,5)* enhanced the association of IGF2BP2 with *CENPB* mRNA, impacting its mRNA stability (Fig. 6l).

Repression of *circMANIA2(2,3,4,5)* induces chromosome instability via *CENPB* mRNA-level modulation

The effect of direct interaction between *circMANIA2(2,3,4,5)* and *CENPB* mRNA on IGF2BP2-mediated *CENPB* mRNA stability (Figs. 5 and 6) suggested the observed effect of *circMANIA2(2,3,4,5)* KD on cell proliferation (Fig. 2) may be due to chromosome instability caused by decreased *CENPB*. By assessing the percentage of bi-nuclei and multi-nuclei during interphase, we found that *circMANIA2(2,3,4,5)* KD significantly increased the incidence of abnormal nuclei in HT29 and DLD-1 (Fig. 7a). As mitotic errors invariably lead to aneuploidy (loss and gain of chromosomes), we further found HT29 and DLD-1, which typically exhibit 60 or 48 chromosomes under stable conditions, respectively, displayed abnormal chromosome numbers with both loss and gain of chromosomes after *circMANIA2(2,3,4,5)* KD (Fig. 7b). In addition, we also observed *circMANIA2(2,3,4,5)* KD resulted in a marked reduction of cells in S phase and a pronounced accumulation in G2/M phase (Fig. 7c and Supplementary Fig. 6a, b).

To further confirm the observed effect of *circMANIA2(2,3,4,5)* KD on cell proliferation was caused by the repression of *CENPB* gene expression, we then re-manipulated *CENPB* expression in the *circMANIA2(2,3,4,5)* KD cells using a *CENPB* overexpression plasmid. As indicated in Fig. 7d, e, overexpression of *CENPB* could rescue the cell cycle arrest (Fig. 7d and Supplementary Fig. 6c) and proliferation deficiency (Fig. 7e) induced by *circMANIA2(2,3,4,5)* KD. These results

align with the roles of *CENPB* in regulating nucleosome assembly and/or stability during mitosis^{60,61}, where *CENPB* depletion results in chromosome mis-segregation, aneuploidy and reduced cell proliferation⁶¹.

LNA targeting the RNA-RNA interaction site on *circMANIA2(2,3,4,5)* inhibits CRC progression

To determine whether *circMANIA2(2,3,4,5)* could be a suitable target for interfering CRC progression, we set to evaluate the observed effect of *circMANIA2(2,3,4,5)* KD on human normal colorectal epithelial cell line (HCoEpiC) and paired normal/CRC organoids.

First, we quantified *circMANIA2(2,3,4,5)* expression in these models. Consistent with its upregulation in CRC, *circMANIA2(2,3,4,5)* levels in CRC cell lines (HT29 and DLD-1) and organoids (#1-CRC and #2-CRC) were two to threefold higher than those in normal HCoEpiC cell line and organoids (#1-Normal and #2-Normal) (Supplementary Fig. 7a).

Next, to examine the functional impact of *circMANIA2(2,3,4,5)* in normal colorectal cells, we performed KD *circMANIA2(2,3,4,5)* using shRNA in HCoEpiC. Both shRNA-c1/c2 effectively reduced *circMANIA2(2,3,4,5)* expression without altering linear *MANIA2* mRNA levels (Supplementary Fig. 7b). However, no significant impact on HCoEpiC proliferation was observed (Supplementary Fig. 7c).

We then extended similar analysis to paired human normal and CRC organoids. *CircMANIA2(2,3,4,5)* KD was achieved in both organoids using the same shRNAs, with minimal impact on linear *MANIA2* (Supplementary Fig. 7d, e). Interestingly, *circMANIA2(2,3,4,5)* KD in normal organoids led to minor suppressive effect on proliferation (Fig. 8a, top panel), and in contrast, a significant inhibition in CRC organoids was observed with *circMANIA2(2,3,4,5)* KD (Fig. 8a, bottom panel).

Finally, we were motivated to explore whether targeting *circMANIA2(2,3,4,5)* could modulate CRC progression. To this end, we designed a further optimized LNA (LNA-*circMANIA2(2,3,4,5)*) ("Methods") that targets the BJS site of *circMANIA2(2,3,4,5)*. LNA-*circMANIA2(2,3,4,5)* significantly suppressed the proliferation of DLD-1 cells, but not HCoEpiC cells, compared to control (Fig. 8b). Moreover, we further applied LNA-*circMANIA2(2,3,4,5)* in xenograft tumor model. After subcutaneously injecting HT29 and DLD-1 cells for 10 days, we started the intra-tumoral injection of LNA-negative control (NC) or LNA-*circMANIA2(2,3,4,5)* and monitored tumor growth every 3 days (Supplementary Fig. 7f). As expected, LNA-*circMANIA2(2,3,4,5)* significantly inhibited xenograft tumor growth of HT29 and DLD-1 cells (Fig. 8c) with significantly reduced tumor size (Fig. 8d) and weight (Fig. 8e). Correspondingly, the LNA-mediated decrease of *circMANIA2(2,3,4,5)* was confirmed by RT-qPCR (Supplementary Fig. 7g), along with decreased expression levels of *CENPB* confirmed by immunofluorescence (IF) (Supplementary Fig. 7h, i). These in vivo results thus suggested the designed LNA targeting the RNA-RNA interaction site could downregulate the expression of *CENPB*, which resulted in the subsequent retardation of CRC progression. Of note,

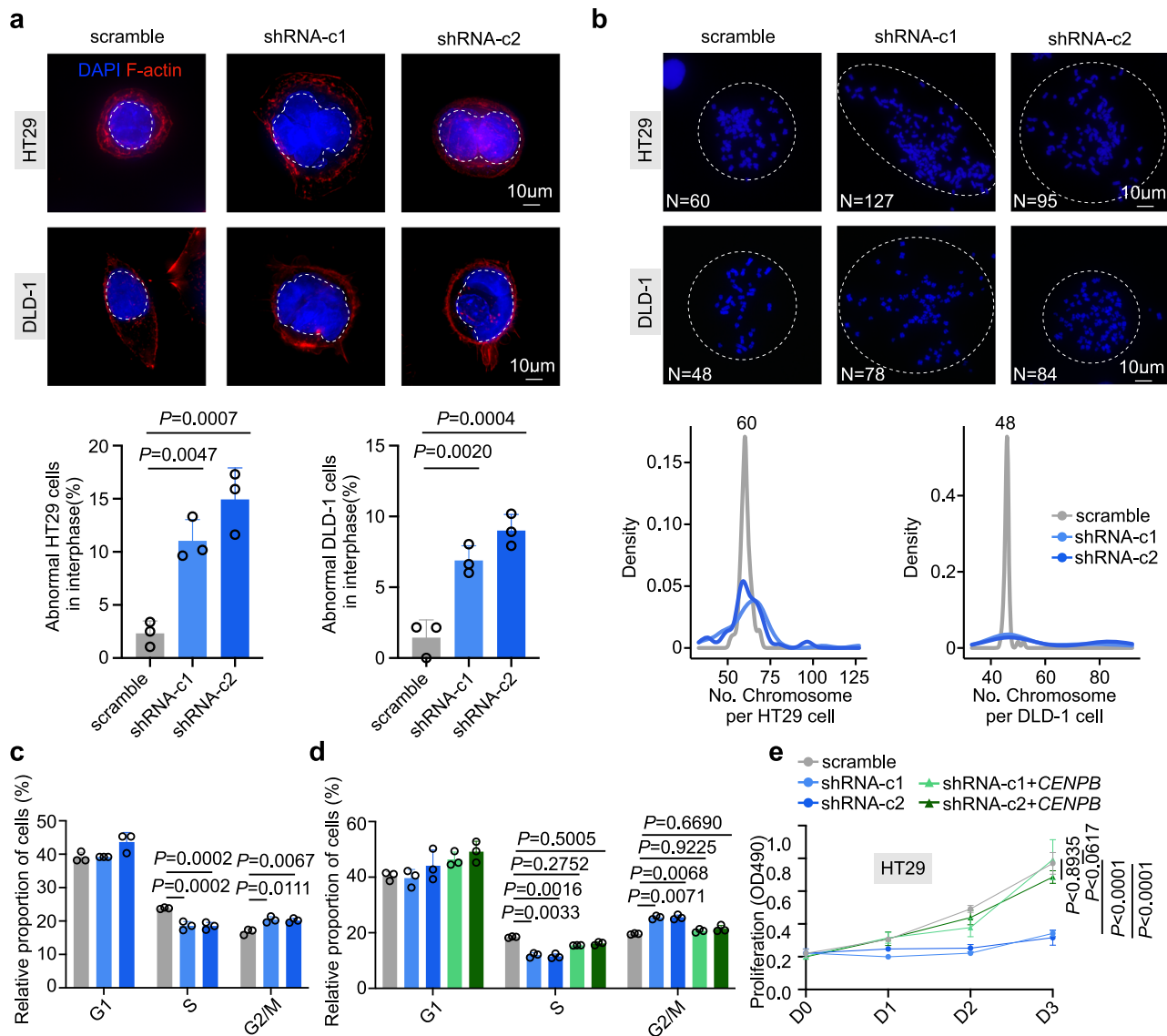


Fig. 7 | Repression of *circMANIA2(2,3,4,5)* induces chromosome instability via *CENPB* mRNA-level modulation. **a, b KD of *circMANIA2(2,3,4,5)* led to binuclei or multinuclei (**a**) and aneuploidy formation (**b**) in *circMANIA2(2,3,4,5)*-KD HT29 and DLD-1 cells. Top, representative images of nuclei (**a**) and chromosomes (**b**), as revealed by immunofluorescent (IF) staining of F-actin (red), nuclei (blue), and chromosomes (blue). Bottom, statistics of abnormal cells percentage in interphase ($n = 60$ cells/independent experiments) (**a**) and chromosome numbers per cell ($n = 60$ cells) (**b**). **c** KD of *circMANIA2(2,3,4,5)* resulted in a marked reduction of cells in S phase and a pronounced accumulation in G2/M phase, as revealed by cell cycle**

analysis. **d, e** Over-expression of *CENPB* rescued the cell cycle (**d**) and proliferation (**e**) deficiency with *circMANIA2(2,3,4,5)* KD, as revealed by cell cycle analysis (**d**) and MTT cell proliferation assay (**e**; $n = 5$ wells of cells examined over three independent experiments). Data are presented as mean \pm s.d. (**a, c–e**), with biologically individual data points shown (**a, c, d**). P values were determined by ordinary one-way ANOVA test with Dunnett's post-hoc comparisons versus scramble control (FDR-adjusted P values) (**a**) and ordinary two-way ANOVA with Dunnett's post-hoc comparisons versus scramble control at each row factor level (adjusted P values) (**c–e**). Source data are provided as a Source Data file.

the reduction of tumor size with LNA treatment were slightly less pronounced than those achieved by shRNAs (Fig. 2i–m), possibly due to the relatively low efficiency of LNA delivery, which requires further investigation.

Discussion

Recent studies have revealed the genome-wide expression of circRNAs produced from pre-mRNA back-splicing of eukaryotic genes. In this study, we further exploited the complexity and diversity of circRNAs by profiling the landscape of AC across different cell lines and paired normal and colon cancer tissues (Fig. 1b and Supplementary Fig. 1). We found that about half of circRNA-producing gene loci could undergo AC to produce multiple circRNA isoforms and a pe-circRNA that accounts to the majority of total FPBs was generally observed at most if

not all AC gene loci (Fig. 1c). Here, we focused on a pe-circRNA, *circMANIA2(2,3,4,5)*, identified at the *MANIA2* gene locus, which was shown to be the top highly expressed circRNA in examined samples and further upregulated in CRC samples (Fig. 1e–h and Supplementary Fig. 2). Moreover, *circMANIA2(2,3,4,5)* KD inhibited cancer cell proliferation and CRC progression (Fig. 2). Detailed studies suggested that *circMANIA2(2,3,4,5)* could directly associate with both IGF2BP2 (Fig. 3) and *CENPB* mRNA (Fig. 6) to regulate *CENPB* mRNA stability (Figs. 4–6), and further to affect chromosome stability (Fig. 7). The applications of LNA (Fig. 8) could significantly inhibit cancer cell proliferation and in vivo tumor growth, but not normal colorectal cells or normal organoids (Fig. 8).

We showed that the direct binding of *circMANIA2(2,3,4,5)* with *CENPB* mRNA is crucial to its specific effect on cancer cell proliferation

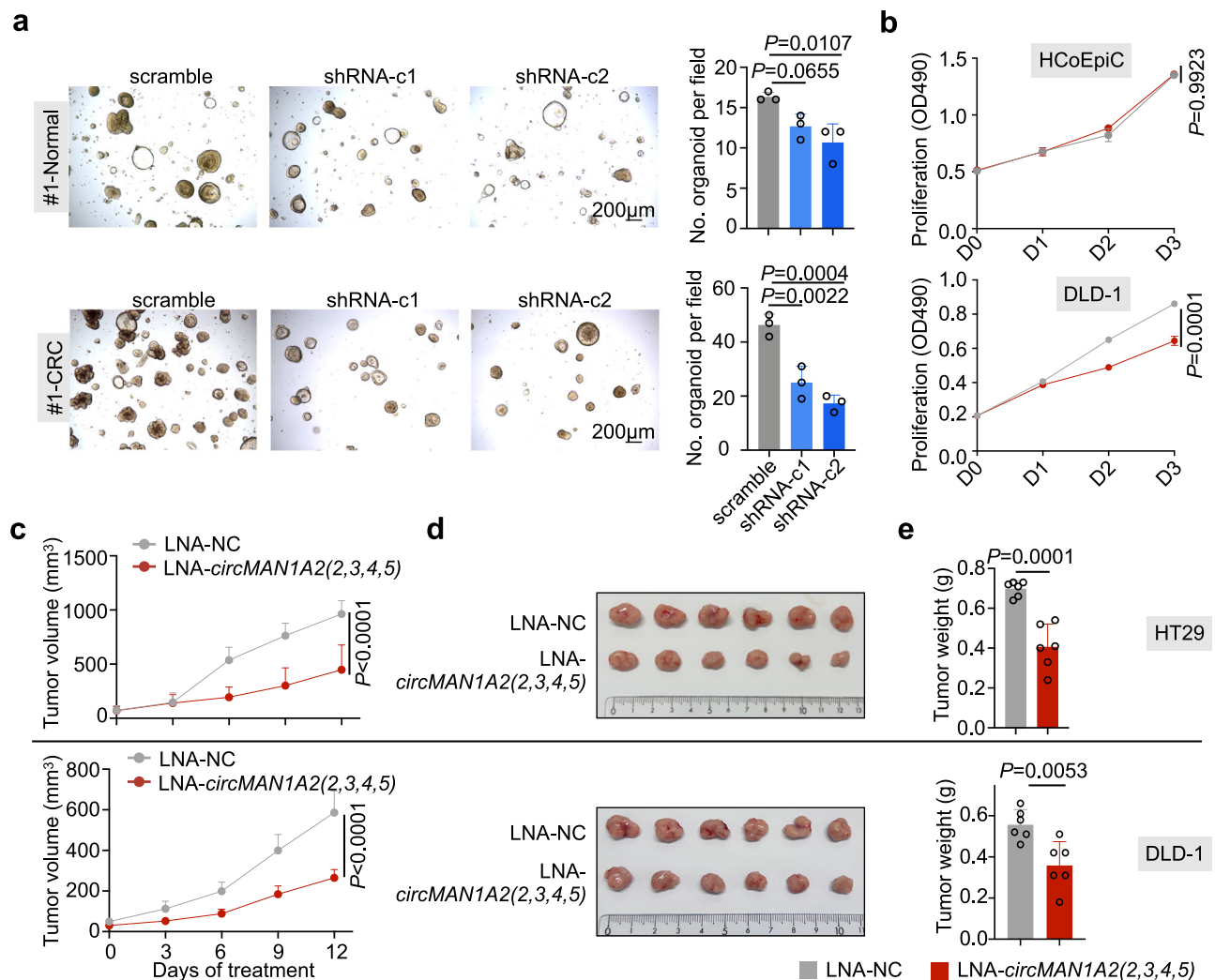


Fig. 8 | LNA targeting the RNA-RNA interaction site on *circMANIA2(2,3,4,5)* inhibits CRC progression. **a** Effects of *circMANIA2(2,3,4,5)* KD on the growth of normal (top panel) and CRC (bottom panel) organoids. Left panel, representative images of organoids from three independent experiments. Right panel, statistics of organoids number per field. **b** Treatment of LNA-*circMANIA2(2,3,4,5)* inhibited cell proliferation of DLD-1 (bottom panel), but not HCoEpiC (top panel) cells, as revealed by MTT cell proliferation assay ($n=5$ wells of cells examined over three independent experiments). **c–e** Tumor growth curves from nude mice injected subcutaneously with HT29 (top panel) and DLD-1 cells (bottom panel), followed by

treating with LNA-NC and LNA-*circMANIA2(2,3,4,5)* were shown in **(c)**; the images of tumors were shown in **(d)**; statistics of tumor weight were shown in **(e)**. Tumor volume was measured every 3 days for 12 days and calculated as $\text{width}^2 \times \text{length} \times 0.5$. $n=6$ biologically independent samples. Data are presented as mean \pm s.d. (**a–c, e**), with biologically individual data points shown (**a, e**). P values were determined by ordinary two-way ANOVA with Dunnett's post-hoc comparisons versus scramble control at each row factor level (adjusted P values) (**b, c**), and unpaired two-tailed Student's t -test (**e**). Source data are provided as a Source Data file.

and tumor progression (Figs. 6–8), possibly due to their much higher *circMANIA2(2,3,4,5)* expression than in normal cell lines and organoids. Indeed, although containing the same primary sequence as its cognate linear *MANIA2* mRNA, the direct binding of *circMANIA2(2,3,4,5)* with *CENPB* mRNA is strictly dependent on its unique BSJ site. Furthermore, we repressed linear *MANIA2* expression (Supplementary Fig. 8a) in both HT29 and DLD-1 cells and found that linear *MANIA2* KD barely affected *CENPB* expression (Supplementary Fig. 8b, c), further supporting the notion that the regulatory effect of *circMANIA2(2,3,4,5)* on *CENPB* mRNA was specifically dependent on their direct binding.

Of note, multiple circRNAs can be produced from the same gene loci through AC, including those from the *MANIA2* gene locus. Additionally, *circMANIA2(2,3,4)* and *circMANIA2(2,3,4,5,6)* were also elevated in colon cancer (Supplementary Fig. 2b), though less than *circMANIA2(2,3,4,5)*. More importantly, the *circMANIA2(2,3,4,5)* BSJ, specifically binding to *CENPB* mRNA, is lacking in the other isoforms. In this scenario, although *circMANIA2(2,3,4)*, but not

circMANIA2(2,3,4,5,6), KD (Supplementary Fig. 8d–f) also inhibited CRC cell proliferation (Supplementary Fig. 8g, h), *circMANIA2(2,3,4)* KD had little effect on *CENPB* expression (Supplementary Fig. 8i). These results together not only illustrate the complex AC expression of the human transcriptome, but also suggest the functional diversity of AC circRNAs, such as on tumor progression.

Interestingly, multiple mouse *circMan1a2* isoforms were also found in the mouse *Man1a2* gene locus and a specific *circMan1a2(2,3,4,5,6)* was demonstrated to be important in mouse embryo preimplantation development³³, while the mouse *circMan1a2(2,3,4,5)* was poorly expressed in the examined mouse embryo RNA-seq samples. Moreover, even though both *circMan1a2(2,3,4,5)* and *circMan1a2(2,3,4,5,6)* were comparably expressed in mouse CRC cell lines (CT26 and MC38), KD of neither *circMan1a2(2,3,4,5)* (Supplementary Fig. 9a) nor *circMan1a2(2,3,4,5,6)* (Supplementary Fig. 9d) affected *Cenpb* expression levels (Supplementary Fig. 9b, c, e, f). Together with the role of *circMANIA2(2,3,4,5)* KD on CRC, but not on normal cell proliferation (Fig. 8), these indicated the regulation of

circMANIA2(2,3,4,5) is also human-specific and not conserved in mice, at least in the context of CRC.

Additionally, while targeting the BSJ of *circMANIA2(2,3,4,5)* can inhibit subcutaneous tumor size (Fig. 8c–e), using LNAs for CRC therapeutics may need further optimization to enhance the in vivo efficacy of LNA-*circMANIA2(2,3,4,5)*. For example: (1) chemical modifications, such as the combination of LNAs with phosphorothioate could bolster oligonucleotide stability and target binding affinity within physiological environments⁶²; (2) length optimization of LNA variants, ranging from 12 to 20 nucleotides, could balance target specificity and binding stability, potentially minimizing off-target effects⁶³; (3) refining target through secondary structure analysis using tools like RNAfold⁹ could identify optimal binding sites within the BSJ region, enhancing accessibility and efficacy; (4) advanced delivery systems, such as tumor-targeted lipid nanoparticles, polymeric carriers or ligand-conjugated formulations, may significantly enhance tumor accumulation and therapeutic efficacy⁶⁴.

Collectively, we report here the profile of the AC landscape across cell lines and tissues, and have identified a specific pe-circRNA, *circMANIA2(2,3,4,5)*, that regulates cell proliferation and CRC progress through its unique BSJ sequence. Delivering specific LNA targeting the *circMANIA2(2,3,4,5)*-BSJ site significantly reduced the tumor progression, suggesting a promising target for CRC. We expect extensive analyses of the genome-wide circRNA expression will reveal other functional circRNAs through AC, benefiting our understanding of the complexity and diversity of human transcriptomes.

Methods

Study approval

Our animal research complies with all relevant ethical regulations according to protocols approved by the Animal Care and Use Committee of Children's Hospital of Fudan University (Approval No. 2024-415). All of the mice were sacrificed and all of the animal experiments were performed under isoflurane anesthesia. Every effort was made to minimize and avoid suffering.

The human organoids used in this study were commercially obtained from D1 Medical Technology (Shanghai, China). The biological source and collection process of the original human tissue samples was reviewed and approved by the Institutional Review Boards of Fudan University Shanghai Cancer Center (2103232-7). The studies were conducted in accordance with recognized ethical guidelines (Declaration of Helsinki). Informed consent was obtained from all of the participants.

Xenograft studies

Mice were housed under controlled conditions with a 12-h light/dark cycle, at an ambient temperature of 20–25 °C and relative humidity of 50 ± 10%. Food and water were available ad libitum. All animals were randomly assigned to experimental groups, and no data points were excluded from the analysis. After transplanted tumor cells, the mice were monitored every three or four days for measuring tumor volume and any signs of suffering or abnormal behavior. Euthanasia was performed via CO₂ inhalation, after which tumors were excised and weighed. In accordance with institutional ethical guidelines, the maximum permitted tumor volume was set at 2500 mm³, and this threshold was not surpassed in any of the experiments.

For assay of the formation of subcutaneous xenograft tumors, 4- to 5-week-old female BALB/c-nude mice (five mice per group) were injected subcutaneously with 1 × 10⁶ HT29 or DLD-1 cells.

As for in vivo-grade LNA targeting, after 4- to 5-week-old female BALB/c-nude mice being injected subcutaneously with 1 × 10⁶ HT29 or DLD-1 cells for 10 days, the mice were randomized for intra-tumoral injection of LNA-NC and LNA-*circMANIA2(2,3,4,5)* (10 nmol per injection, once per three days). In vivo-grade LNA-*circMANIA2(2,3,4,5)* were designed and synthesized by RIBOBIO (Guangzhou, China).

LNAs used in this work were listed in Supplementary Data 6.

For assay of the formation of orthotopically xenograft tumor model was constructed as previously described⁴⁴. Briefly, 4- to 5-week-old female NSG mice were anesthetized with tribromoethanol solution and 2 × 10⁶ HT29 or DLD-1 cells were injected into the wall of the cecum. Then the mice were closed using sterile suture.

Cell lines and cell culture

Human HeLa and HEK293FT cells were purchased from the American Type Culture Collection (ATCC; <http://www.atcc.org>). HT29, DLD-1, CT26, MC38 and A549 cells were purchased from National Collection of Authenticated Cell Cultures. HCoEpiC cell was purchased from Bluefbio (Shanghai) Biology Technology Development Co., Ltd. Normal and CRC organoids (sample #1 and #2) were derived from female and male donors, respectively, and obtained from D1 Medical Technology (Shanghai, China). All cells were originally authenticated using Short tandem repeat profiling.

HeLa, HEK293FT, A549 and HCoEpiC cells were maintained in DMEM supplemented with 10% Fetal Bovine Serum (FBS). HT29, DLD-1, CT26 and MC38 were maintained in RPMI-1640 supplemented with 10% FBS. Organoids were maintained in commercial colorectal organoid amplification medium (D1 Medical Technology, K212M02-1). All cell lines were cultured at 37 °C with 5% CO₂, and were routinely screened to exclude mycoplasma contamination.

Cell transfection and lentivirus infection

Human cell lines and organoids were maintained and passaged following the standard procedures recommended by the ATCC and D1 Medical Technology. Plasmid or LNA transfections were performed using Lipofectamine 3000 (Cat# L3000015, Invitrogen) or RNAiMAX Transfection Reagent (Cat# 13778150, Invitrogen), respectively, in accordance with the manufacturer's instructions.

To produce lentiviral particles, HEK293FT cells (60%–70% confluence) were co-transfected with main construct, psPAX2, and pMD2.G. The supernatant containing viral particles was collected, filtered, and stored at –80 °C till use. To increase the infection efficiency, cells were cultured with medium containing lentivirus and 10 µg ml⁻¹ polybrene. Two days later, infected cells were selected with 2 µg ml⁻¹ puromycin.

Northern blot (NB)

Northern blotting was performed using the DIG Northern Starter Kit (Cat# 12039672910, Roche) following the manufacturer's instructions. Total RNA (5 µg) was resolved on a 1% agarose or denaturing PAGE gel by electrophoresis (120 V, 2 h, 4 °C) and transferred to a nylon membrane (Roche) either at 20 V for 20 h or 400 mA for 90 min at 4 °C. Membranes were UV cross-linked, prehybridized in DIG Easy Hyb (68 °C, 2 h), and hybridized overnight (68 °C, 16 h) with 800 ng DIG-labeled RNA probe. The following day, membranes were washed twice at room temperature with 2× SSC/0.1% SDS (5 min each), followed by two washes at 68 °C for 30 min in 0.2× SSC/0.1% SDS. Subsequently, they were rinsed for 5 min at room temperature in washing buffer (0.3% Tween-20 in 1× maleic acid buffer) and blocked for 30 min in 1× blocking buffer. Meanwhile, Anti-DIG-AP antibody (Roche) was diluted in 1× blocking buffer. After blocking, membranes were incubated with the diluted antibody for 30 min at room temperature, washed three times (20 min each) with washing buffer, and equilibrated in 1× detection buffer before signal development. Signals were detected using CDP-Star (Roche) and imaged with a chemiluminescence system.

All primers used for making probes were listed in Supplementary Data 6.

Cell proliferation assay

Cell proliferation was detected by an MTT assay that measures OD₄₉₀ according to manufacturer's protocol of CellTiter 96 Aqueous One

Solution Cell Proliferation Assay (Promega). We seeded 3×10^3 or 5×10^3 DLD-1 or HT29 cells per well into 96-well dishes, then cultured these at 37 °C in a 5% CO₂ cell-culture incubator until the indicated time points. Live cells at day 0, day 1, day 2, and day 3 were detected by MTT at corresponding time points. Data were normalized to the value at day 0.

Western Blot

Cell lysates were prepared with 1× SDS loading buffer, separated by SDS-PAGE, and transferred to a 0.22 μm PVDF membrane. Membranes were blocked at room temperature for 1 h in 5% BSA dissolved in PBST (PBS containing 0.1% Tween-20), followed by primary antibodies overnight incubation at 4 °C. After three 10-min washes with PBST, membranes were incubated with secondary antibodies for 1 h at room temperature, washed again three times with PBST, and then incubated with the ECL dection buffers (Cat#34580, Thermo Fisher Scientific). The protein signals were detected via Tanon 5200 Chemiluminescence Imaging System.

Primary antibodies used were anti-β-actin (1:5000, Cat# A3854, Sigma), anti-FLAG (1:5000, Cat# F1804, Sigma), anti-GAPDH (1:5000, Cat#AB0038, Abways), anti-Histone H3 (1:5000, Cat# ab1791, Abcam), anti-CENPB (1:1000, Cat# ab259855, Abcam), anti-IGF2BP2 (1:1000, Cat# ab124930, Abcam) and anti-MANIA2 (1:1000, Cat# ab272611, Abcam).

RNA isolation, RT-qPCR

Total RNAs were extracted with Trizol Reagent (Cat# 15596018, Ambion). The reverse transcription and RT-qPCR was carried out using PrimeScript RT Master Mix (Cat# RRO36A, TaKaRa) and SYBR Green Realtime PCR Master Mix (Cat# QPS-201C, TOYOBO). The relative expression of different sets of genes was quantified to *GAPDH* or *ACTIN* mRNA.

Cytoplasmic and nuclear RNA fractionation in HT29 cells was carried out based on a previously reported protocol³³ with modifications. Briefly, 1×10^6 cells were washed twice with ice-cold PBS and pelleted by centrifugation at $120 \times g$ for 3 min. The cell pellet was gently resuspended in 200 μL lysis buffer containing 10 mM Tris-HCl (pH 8.0), 140 mM NaCl, 1.5 mM MgCl₂, 0.5% Igepal, and 2 mM Ribonucleoside Vanadyl Complex. Following lysis, the suspension was centrifuged at $1000 \times g$ for 3 min at 4 °C to separate nuclei (pellet) from cytoplasmic components (supernatant). The cytoplasmic fraction was further clarified by centrifugation at $1000 \times g$ for 10 min at 4 °C. The nuclear pellet was washed once with 200 μL lysis buffer containing 0.5% deoxycholic acid to reduce cytoplasmic contamination. Finally, both cytoplasmic and nuclear fractions were subjected to RNA extraction and reverse transcription, followed by RT-qPCR analysis.

All primers used for RT-qPCR were listed in Supplementary Data 6.

In vitro RNA transcription, circularization, and purification

CircRNAs were generated by in vitro transcription from 1 μg of linearized T7-driven plasmids in a 20 μL reaction using the RiboMax system (Promega), following the manufacturer's instructions. To promote circularization, 0.5 μL of 1 M MgCl₂ was added after transcription. Residual DNA templates were eliminated by treatment with 1 μL Turbo DNase I at 37 °C for 15 min. The synthesized RNAs were purified by ethanol precipitation and resuspended in RNase/DNase-free water. A portion of the RNA samples was treated with RNase R at 37 °C for 45 min. Subsequently, all RNA samples were analyzed by urea-PAGE. Target RNA bands were excised, eluted into TE buffer, and recovered through ethanol precipitation, followed by dissolution in RNase/DNase-free water. Purified RNAs were stored at -80 °C until further use.

Primers for circularization were listed in Supplementary Data 6.

Electrophoretic mobility shift assay (EMSA)

Dig-labeled RNAs were first denatured at 65 °C for 5 min and then gradually cooled to room temperature to allow annealing. For binding assays, 1 pmol of the labeled RNA was incubated with the indicated concentration of purified protein in binding buffer (100 mM HEPES, pH 7.5; 10 mM DTT; 10 mM MgCl₂; 200 mM KCl) for 25 min. The reaction mixtures were directly resolved on a 5% native PAGE gel, which was run at 130 V for 2 h. After electrophoresis, gels were stained with SYBR Green II for 20 min, and RNA signals were visualized using FLA-9000.

RNA immunoprecipitation (RIP)

HT29 cells were collected from 10-cm dishes, lysed in RIP buffer (50 mM Tris-HCl, pH 8.0; 150 mM NaCl; 0.5% Igepal; 1 mM PMSF; protease inhibitors; 2 mM RVC) by mild sonication, and cleared by centrifugation. Supernatants were precleared with Dynabeads Protein G (Invitrogen) before immunoprecipitation with anti-IGF2BP2 or control IgG antibodies (Abcam) at 4 °C for 2 h. Beads were washed with high-salt and RIP buffers, and bound complexes were eluted in elution buffer (100 mM Tris, pH 6.8, 4% SDS, and 10 mM EDTA). A portion of the eluate was analyzed by WB, while the rest was processed for RNA extraction and RT-qPCR.

Biotin-labeled RNA pull-down, silver staining, and mass spectrometry

For in-cell RNA pull-down, biotin-labeled RNAs (4 μg) were heated for 5 min at 65 °C in PA buffer (10 mM Tris-HCl pH 7.5, 10 mM MgCl₂, 100 mM NH₄Cl) and slowly cooled down to room temperature. To prepare cell lysate for pull-down with *lucMANIA2(2,3,4,5)*, linear *MANIA2(2,3,4,5)* or single-stranded (ss) RNA (*EGFP*), 1×10^7 HT29 or DLD-1 cells were resuspended in 1 mL binding buffer (100 mM HEPES pH 7.0, 50 mM KCl, 10% glycerol, 1 mM EDTA, 1 mM DTT, 0.5% Triton ×100) supplemented with tRNA (0.1 mg/ml), heparin (0.5 mg/ml) and RNasin (1 unit/μl). The cell lysates were sonicated and centrifuged at $14,000 \times g$ for 10 min at 4 °C. The supernatant was pre-cleared with MyOne Streptavidin C1 beads (Cat# 65001, Invitrogen) for 30 min at 4 °C, followed by incubation with folded RNAs for 2 h and with beads for 1 h at 4 °C. Beads were washed five times with the binding buffer, and boiled in 1× sample buffer for 10 min. The retrieved proteins were subjected to NuPAGE 4%–12% Bis-Tris Gel (Invitrogen). Then proteins were visualized using the Pierce™ Silver Stain for Mass Spectrometry kit (Cat# 24600, Thermo Fisher Scientific) according to the manufacturer's instructions. Target protein bands were excised and subjected to in-gel tryptic digestion at 37 °C for 20 h. Gel fragments were processed by Applied Protein Technology (Shanghai) for nanoLC-MS/MS analysis on a Q Exactive™ Hybrid Quadrupole-Orbitrap mass spectrometer (Thermo Fisher Scientific) coupled to an EASY-nLC™ 1200 system (Thermo Fisher Scientific). Raw spectra were processed using Proteome Discoverer™ 2.5 (Thermo Fisher Scientific) against the UniProt *Homo sapiens* reference proteome (release 2021_04, 20,386 entries). Identified proteins by MS are listed in Supplementary Data 4.

For in vitro RNA pull-down, the cell lysates of HT29 and DLD-1 cells were replaced with purified IGF2BP2 protein from *E. coli*. The following processes were similar to in-cell RNA pull-down.

For LNA-blocked RNA pull-down, biotin-labeled RNAs were first annealed with individual LNAs (LNA-blocked) at a molar ratio of 1:5. The following processes were similar to in vitro RNA pull-down.

LNAs used in this work were listed in Supplementary Data 6.

RNA-RNA interaction assay

For psoralen-crosslinked RNA-RNA interaction assay, which was performed as described⁵⁸ with modifications, 1×10^7 HT29 or DLD-1 cells were resuspended in cold PBS with 200 μg/ml AMT (Cat# 81010, Sigma) and irradiated at 365 nm with a Spectroline ENF-280C UV lamp

at an intensity of approximately 100 mW/cm² for five 2-min cycles. 1 volume of 6M Guanidinium Hydrochloride was added to 1 volume of AMT. The lysate was subdivided into 250 μ L aliquots. To each aliquot, 25 μ L of a 20 mg/mL solution of Proteinase K (Ambion) and 6.5 μ L of 20% SDS were added. The samples were then incubated at 65 °C for 1 h. RNA was precipitated with TRIzol and the protocol proceeded as previously described. RNA was resuspended in 500 μ L of H₂O, denatured at 95 °C for 3 min, and immediately transferred to ice. 500 pmol of biotinylated probe were added to each sample and incubated at 65 °C for 5 min and 500 μ L of 2 \times binding buffer heated at 65 °C was added to each sample. A 100 μ L aliquot was set aside as input control; the remaining mixture was rotated continuously for 4 h at room temperature. Add 125 μ L MyOne Streptavidin C1 beads and incubated overnight at 4 °C and washed twice with 1 \times binding buffer and twice with 1 \times wash buffer. RNA bound to the beads was extracted using 1 mL of TRIzol. The purified RNA was resuspended in 25 μ L of H₂O and dispensed onto a parafilm-covered glass plate resting on ice. To reverse AMT crosslinks, samples were directly irradiated with 254 nm UV light for 10 min. After irradiation, the samples were pooled and brought to a final volume of 300 μ L with water. RNA was precipitated overnight at -20 °C by adding 2 μ L glycogen, 30 μ L of 3M sodium acetate (pH 5.2), and 900 μ L absolute ethanol. Enrichment of target RNA was evaluated by RT-qPCR.

For in vitro RNA pull-down, the cell lysate of HT29 and DLD-1 cells was replaced with *CENPB*-CDS or *CENPB*-3'UTR. The following processes were similar to in-cell RNA pull-down.

For LNA-blocked RNA pull-down, biotin-labeled RNAs were first annealed with individual LNAs (LNA-blocked) at a molar ratio of 1:5. The following processes were similar to in vitro RNA pull-down.

LNAs used in this work were listed in Supplementary Data 6.

Measurement of RNA copy number

Absolute quantification of *circMANIA2(2,3,4,5)* and *CENPB* mRNA was performed by RT-qPCR using serial dilutions of in vitro-transcribed RNAs to generate standard curves. Copy numbers were calculated with a DNA/RNA copy number calculator. For cell-based quantification, total RNA from 1 \times 10⁶ HT29 or DLD-1 cells was reverse transcribed into cDNA, and RNA copy numbers were determined according to the standard curves.

Cell cycle analysis

Cells (1 \times 10⁶ per well) were seeded in 6-well plates and cultured for 24 h. Subsequently, they were pulsed with 10 μ M 5-ethynyl-2'-deoxyuridine (EdU) at 37 °C for 30 min, followed by staining with Click-iT™ EdU Alexa Fluor™ 647 Flow Cytometry Assay Kit (Cat# C10424, Thermo Fisher Scientific) according to the manufacturer's protocol. DNA content was quantified using DAPI (0.5 μ g/mL). Flow cytometric data were analyzed with FlowJo software.

RNA library construction and sequencing

Total RNA was subjected to rRNA depletion using the KAPA RiboErase Kit (HMR). Next, ribo- RNA-seq libraries were constructed with the KAPA RNA HyperPrep Kit (Roche) and purified by size selection with KAPA Pure Beads (Roche). Library quality and concentration were assessed with an Agilent 2100 Bioanalyzer and a Qubit dsDNA HS Assay Kit (ABP Biosciences). Sequencing was performed on an Illumina NovaSeq 6000 platform at Sequanta Technologies, Shanghai, China.

All the above raw read qualities were evaluated by FastQC (<http://www.bioinformatics.babraham.ac.uk/projects/fastqc/>).

Pipeline for ribo- RNA-seq data processing

Raw ribo- RNA-seq reads were cleaned using trimmomatic⁶⁵ to eliminate adaptor sequences and low-quality bases. For linear RNA quantification, the filtered reads were aligned to the human reference genome GRCh38/hg38 with GENCODE annotation (version 41) using

HISAT2⁶⁶. The resulting alignments were then converted to BAM files using samtools⁶⁷. FPKM⁶⁸ (Fragments Per Kilobase of transcript per Million mapped reads) was used to quantify gene expression levels. CircRNA abundance was assessed as FPB (Fragments Per Base) using CIRCexplorer3/CLEAR²⁹.

Differential circRNA expression analysis between normal control and colon cancer samples

The circRNA expression levels in ribo- RNA-seq data from 20 paired normal control and colon cancer samples were first quantified by CIRCexplorer3/CLEAR and further summarized into a BSJ-read count matrix. This matrix was computed as Counts Per Million (CPM) and then used for differentially expressed circRNAs analysis with edgeR (version 3.28.1)⁵¹. CircRNAs were defined as upregulated when the FC (CPM_{colon_cancer}/CPM_{normal_control}) was ≥ 1.5 with the false discovery rate (FDR) < 0.01 and as downregulated when the FC was ≤ 0.667 with the FDR < 0.01. The resulting differentially expressed circRNAs are shown in Fig. 1e.

Analysis of differentially expressed genes upon *circMANIA2(2,3,4,5)* knockdown

Following the processing of ribo- RNA-seq data, gene-level counts were obtained from six samples for each examined cell line: including scramble rep1, *circMANIA2(2,3,4,5)* shRNA-c1 rep1, *circMANIA2(2,3,4,5)* shRNA-c2 rep1, scramble rep2, *circMANIA2(2,3,4,5)* shRNA-c1 rep2, and *circMANIA2(2,3,4,5)* shRNA-c2 rep2. Similar to the differential circRNA expression analysis, this matrix was computed as CPM and subsequently used to identify differentially expressed genes with edgeR⁵¹. Genes were defined as upregulated when the FC (CPM_{shRNA}/CPM_{scramble}) was ≥ 1.5 with the FDR < 0.01, and as downregulated when the FC was ≤ 0.667 with the FDR < 0.01. Volcano plots of DEGs for the five examined cell lines were presented in Supplementary Fig. 4a. Overlapping DEGs in both shRNA-c1 and shRNA-c2 groups were listed in Supplementary Fig. 4b.

Quantification of circRNAs in exome capture RNA-seq data

All circRNA and their cognate linear RNA abundances for the COLO, OV, LUAD, PRAD, AML, and BRCA cohorts were downloaded from the MiOncoCirc database³⁹ (<https://mioncocirc.github.io/>). Since these circRNA abundances were identified using exome capture RNA-seq data, we employed the “normalized read count” to assess circRNA expression levels, as described in the previous study³⁹. This method normalizes back-spliced reads to the median mapped reads of all libraries in the cohorts. Specifically, in our selected cohorts, one “normalized read count” corresponds to one back-spliced read per 50 million mapped reads of linear genes. Of note, we only included high-confidence circRNAs that appeared in at least five samples and had an average of more than one normalized read count for subsequent analysis.

Identification of *ivcMANIA2(2,3,4,5)*-enriched proteins from MS results

Based on the MS results from *ivcMANIA2(2,3,4,5)* rep1, *ivcMANIA2(2,3,4,5)* rep2, *EGFP* rep1, and *EGFP* rep2, proteins with at least one unique peptide in both replicates of either *ivcMANIA2(2,3,4,5)* or *EGFP* group were retained for analysis. The FC in abundance (abundance_{*ivcMANIA2(2,3,4,5)*}/abundance_{*EGFP*}) and corresponding *P* values were then computed. A cutoff of FC > 2 and *P* value < 0.05 was applied to define *ivcMANIA2(2,3,4,5)*-enriched proteins. The volcano plot of *ivcMANIA2(2,3,4,5)*-enriched proteins was shown in Fig. 3b.

Prediction of RNA-RNA interacting regions between *circMANIA2(2,3,4,5)* and *CENPB* mRNA

As reported by the previous study⁶⁹, we used *CENPB* mRNA sequence and the exonic *circMANIA2(2,3,4,5)* sequence with additionally

extended sequence of exon2, to include the region around the BSJ as input, to predict their binding regions using IntaRNA version 3.3.2⁵⁹. The predict result with the lowest minimum free energy was shown in Fig. 6e.

Statistical analysis

Data in this study were presented as mean ± standard deviation (s.d.). Error bars represented s.d. in three biologically independent experiments if not mentioned otherwise. For comparisons between two groups with normally distributed data, an unpaired two-tailed Student's *t*-test was applied. For multiple-group comparisons with non-normally distributed data, nonparametric ordinary one-way or two-way ANOVA with Dunnett's post-hoc test was employed. For transcriptome analyses, statistical significance was determined with a two-tailed Welch's *t*-test. GO analysis significance was computed using a one-tailed hypergeometric test implemented in R (version 3.6.0). All inclusion and exclusion criteria were predetermined and no samples or animals were excluded from analysis. Experiments were randomized and investigators were blinded to allocation throughout the experiments and when analyzing the results and each experiment was repeated independently at least three times with similar results.

Reporting summary

Further information on research design is available in the Nature Portfolio Reporting Summary linked to this article.

Data availability

The ribo- RNA-seq data of HT29, DLD-1, LoVo, HeLa, A549, and 293FT cell lines generated in this study have been deposited in the Gene Expression Omnibus (GEO) database under the accession code [GSE274247](https://www.ncbi.nlm.nih.gov/geo/query/acc.cgi?acc=GSE274247). The paired ribo- RNA-seq data of normal and colon cancer samples from patients were previously published³⁰ and are available in the Genome Sequence Archive for Human (GSA-Human) database under the accession code PRJCA001113 after request (<https://ngdc.cncb.ac.cn/gsa-human/browse/HRA000037>). The exome capture RNA-seq data from COLO, OV, LUAD, PRAD, AML, and BRCA various cancer tissues used in this study are available in the MiOncoCirc database³⁹ (<https://mioncocirc.github.io/>). The raw protein mass spectrometry data have been deposited in the Integrated Proteome Resources (iProX) database under the accession code [IPX0010131000](https://www.iprox.org/). Source data are provided with this paper.

References

- Chen, L. L. The biogenesis and emerging roles of circular RNAs. *Nat. Rev. Mol. Cell Biol.* **17**, 205–211 (2016).
- Kristensen, L. S. et al. The biogenesis, biology and characterization of circular RNAs. *Nat. Rev. Genet.* **20**, 675–691 (2019).
- Chen, L. L. The expanding regulatory mechanisms and cellular functions of circular RNAs. *Nat. Rev. Mol. Cell Biol.* **21**, 475–490 (2020).
- Liu, C. X. & Chen, L. L. Circular RNAs: characterization, cellular roles, and applications. *Cell* **185**, 2016–2034 (2022).
- Yang, L., Wilusz, J. E. & Chen, L. L. Biogenesis and regulatory roles of circular RNAs. *Annu. Rev. Cell Dev. Biol.* **38**, 263–289 (2022).
- Zhang, Y. et al. Circular intronic long noncoding RNAs. *Mol. Cell* **51**, 792–806 (2013).
- Gu, Y. et al. Circular RNA circIPO11 drives self-renewal of liver cancer initiating cells via Hedgehog signaling. *Mol. Cancer* **20**, 132 (2021).
- Conn, V. M. et al. A circRNA from SEPALLATA3 regulates splicing of its cognate mRNA through R-loop formation. *Nat. Plants* **3**, 17053 (2017).
- Hansen, T. B. et al. Natural RNA circles function as efficient micro-RNA sponges. *Nature* **495**, 384–388 (2013).
- Barrett, S. P., Parker, K. R., Horn, C., Mata, M. & Salzman, J. ciRS-7 exonic sequence is embedded in a long non-coding RNA locus. *PLoS Genet.* **13**, e1007114 (2017).
- Memczak, S. et al. Circular RNAs are a large class of animal RNAs with regulatory potency. *Nature* **495**, 333–338 (2013).
- Xia, P. et al. A circular RNA protects dormant hematopoietic stem cells from DNA sensor cGAS-mediated exhaustion. *Immunity* **48**, 688–701.e687 (2018).
- Chen, C. K. et al. Structured elements drive extensive circular RNA translation. *Mol. Cell* **81**, 4300–4318.e4313 (2021).
- Pamudurti, N. R. et al. Translation of CircRNAs. *Mol. Cell* **66**, 9–21.e27 (2017).
- Legnini, I. et al. Circ-ZNF609 is a circular RNA that can be translated and functions in myogenesis. *Mol. Cell* **66**, 22–37.e29 (2017).
- Yang, Y. et al. Extensive translation of circular RNAs driven by N(6)-methyladenosine. *Cell Res.* **27**, 626–641 (2017).
- Guarnerio, J. et al. Oncogenic role of fusion-circRNAs derived from cancer-associated chromosomal translocations. *Cell* **165**, 289–302 (2016).
- Li, Q. et al. CircACC1 regulates assembly and activation of AMPK complex under metabolic stress. *Cell Metab.* **30**, 157–173.e157 (2019).
- Smid, M. et al. The circular RNome of primary breast cancer. *Genome Res.* **29**, 356–366 (2019).
- Rybak-Wolf, A. et al. Circular RNAs in the mammalian brain are highly abundant, conserved, and dynamically expressed. *Mol. Cell* **58**, 870–885 (2015).
- You, X. et al. Neural circular RNAs are derived from synaptic genes and regulated by development and plasticity. *Nat. Neurosci.* **18**, 603–610 (2015).
- Li, X. et al. Coordinated circRNA biogenesis and function with NF90/NF110 in Viral Infection. *Mol. Cell* **67**, 214–227.e217 (2017).
- Liu, C. X. et al. Structure and degradation of circular RNAs regulate PKR activation in innate immunity. *Cell* **177**, 865–880.e821 (2019).
- Zhang, X. O. et al. Complementary sequence-mediated exon circularization. *Cell* **159**, 134–147 (2014).
- Zhang, X. O. et al. Diverse alternative back-splicing and alternative splicing landscape of circular RNAs. *Genome Res.* **26**, 1277–1287 (2016).
- Chen, L. L. et al. A guide to naming eukaryotic circular RNAs. *Nat. Cell Biol.* **25**, 1–5 (2023).
- Ma, X. K., Zhai, S. N. & Yang, L. Approaches and challenges in genome-wide circular RNA identification and quantification. *Trends Genet.* **39**, 897–907 (2023).
- Vromman, M. et al. Large-scale benchmarking of circRNA detection tools reveals large differences in sensitivity but not in precision. *Nat. Methods* **20**, 1159–1169 (2023).
- Ma, X. K. et al. CIRCexplorer3: a CLEAR pipeline for direct comparison of circular and linear RNA expression. *Genomics Proteom. Bioinforma.* **17**, 511–521 (2019).
- Ju, H. Q. et al. A circRNA signature predicts postoperative recurrence in stage II/III colon cancer. *EMBO Mol. Med.* **11**, e10168 (2019).
- Guo, R. et al. CircMAN1A2 is upregulated by *Helicobacter pylori* and promotes development of gastric cancer. *Cell Death Dis.* **13**, 409 (2022).
- Li, Y., Liu, J., Luo, R., You, Y. & Chen, G. Circ-MAN1A2 contributes to the acquired resistance of gefitinib by binding to miR-409-3p to induce TWIST1 expression in non-small-cell lung cancer. *Bio-technol. Bioprocess Eng.* **27**, 556–571 (2022).
- Li, S. et al. Screening for functional circular RNAs using the CRISPR-Cas13 system. *Nat. Methods* **18**, 51–59 (2021).

34. Liu, G. et al. Cancer-associated fibroblast-derived CXCL11 modulates hepatocellular carcinoma cell migration and tumor metastasis through the circUBAP2/miR-4756/IFIT1/3 axis. *Cell Death Dis.* **12**, 260 (2021).
35. Wang, Y., Li, X., Wang, H. & Zhang, G. CircCAMSAP1 promotes non-small cell lung cancer proliferation and inhibits cell apoptosis by sponging miR-1182 and regulating BIRC5. *Bioengineered* **13**, 2428–2439 (2022).
36. Zhang, S. et al. A novel protein encoded by circRsrc1 regulates mitochondrial ribosome assembly and translation during spermatogenesis. *BMC Biol.* **21**, 94 (2023).
37. Zhou, C. et al. circCAMSAP1 promotes tumor growth in colorectal cancer via the miR-328-5p/E2F1 axis. *Mol. Ther.* **28**, 914–928 (2020).
38. Huang, D. et al. Geographic encoding of transcripts enabled high-accuracy and isoform-aware deep learning of RNA methylation. *Nucleic Acids Res.* **50**, 10290–10310 (2022).
39. Vo, J. N. et al. The landscape of circular RNA in cancer. *Cell* **176**, 869–881.e813 (2019).
40. Dang, Q. Q. et al. CircMAN1A2 contributes to nasopharyngeal carcinoma progression via enhancing the ubiquitination of ATMIN through miR-135a-3p/UBR5 axis. *Hum. Cell* **36**, 657–675 (2023).
41. Fan, C. M. et al. circMAN1A2 could serve as a novel serum biomarker for malignant tumors. *Cancer Sci.* **110**, 2180–2188 (2019).
42. Khong, A. et al. The stress granule transcriptome reveals principles of mRNA accumulation in stress granules. *Mol. Cell* **68**, 808–820.e805 (2017).
43. Raj, A., van den Bogaard, P., Rifkin, S. A., van Oudenaarden, A. & Tyagi, S. Imaging individual mRNA molecules using multiple singly labeled probes. *Nat. Methods* **5**, 877–879 (2008).
44. Zhang, L. & Bu, P. Generation of an orthotopic mouse model to study colorectal cancer metastasis. *STAR Protoc.* **2**, 100792 (2021).
45. Gao, X. et al. Circular RNA-encoded oncogenic E-cadherin variant promotes glioblastoma tumorigenicity through activation of EGFR-STAT3 signalling. *Nat. Cell Biol.* **23**, 278–291 (2021).
46. Huang, W. et al. TransCirc: an interactive database for translatable circular RNAs based on multi-omics evidence. *Nucleic Acids Res.* **49**, D236–d242 (2021).
47. Guo, S. K. et al. Therapeutic application of circular RNA aptamers in a mouse model of psoriasis. *Nat. Biotechnol.* **43**, 236–246 (2024).
48. Liu, C. X. et al. RNA circles with minimized immunogenicity as potent PKR inhibitors. *Mol. Cell* **82**, 420–434.e426 (2022).
49. Huang, H. et al. Recognition of RNA N(6)-methyladenosine by IGF2BP proteins enhances mRNA stability and translation. *Nat. Cell Biol.* **20**, 285–295 (2018).
50. Weng, H. et al. The m(6)A reader IGF2BP2 regulates glutamine metabolism and represents a therapeutic target in acute myeloid leukemia. *Cancer Cell* **40**, 1566–1582.e1510 (2022).
51. Robinson, M. D., McCarthy, D. J. & Smyth, G. K. edgeR: a Bioconductor package for differential expression analysis of digital gene expression data. *Bioinformatics* **26**, 139–140 (2010).
52. Carroll, C. W., Silva, M. C., Godek, K. M., Jansen, L. E. & Straight, A. F. Centromere assembly requires the direct recognition of CENP-A nucleosomes by CENP-N. *Nat. Cell Biol.* **11**, 896–902 (2009).
53. McKinley, K. L. & Cheeseman, I. M. The molecular basis for centromere identity and function. *Nat. Rev. Mol. Cell Biol.* **17**, 16–29 (2016).
54. Black, B. E. & Cleveland, D. W. Epigenetic centromere propagation and the nature of CENP-a nucleosomes. *Cell* **144**, 471–479 (2011).
55. Gordon, D. J., Resio, B. & Pellman, D. Causes and consequences of aneuploidy in cancer. *Nat. Rev. Genet.* **13**, 189–203 (2012).
56. Lengauer, C., Kinzler, K. W. & Vogelstein, B. Genetic instabilities in human cancers. *Nature* **396**, 643–649 (1998).
57. Zhang, Y. et al. Optimized RNA-targeting CRISPR/Cas13d technology outperforms shRNA in identifying functional circRNAs. *Genome Biol.* **22**, 41 (2021).
58. Gorbea, C., Mosbrugger, T. & Cazalla, D. A viral Sm-class RNA base-pairs with mRNAs and recruits microRNAs to inhibit apoptosis. *Nature* **550**, 275–279 (2017).
59. Mann, M., Wright, P. R. & Backofen, R. IntaRNA 2.0: enhanced and customizable prediction of RNA-RNA interactions. *Nucleic Acids Res.* **45**, W435–W439 (2017).
60. Blower, M. D. & Karpen, G. H. The role of Drosophila CID in kinetochore formation, cell-cycle progression and heterochromatin interactions. *Nat. Cell Biol.* **3**, 730–739 (2001).
61. Fachinetti, D. et al. DNA sequence-specific binding of CENP-B enhances the fidelity of human centromere function. *Dev. Cell* **33**, 314–327 (2015).
62. Kurreck, J., Wyszko, E., Gillen, C. & Erdmann, V. A. Design of anti-sense oligonucleotides stabilized by locked nucleic acids. *Nucleic Acids Res.* **30**, 1911–1918 (2002).
63. Katayama, S. et al. Antisense transcription in the mammalian transcriptome. *Science* **309**, 1564–1566 (2005).
64. Whitehead, K. A. et al. Degradable lipid nanoparticles with predictable in vivo siRNA delivery activity. *Nat. Commun.* **5**, 4277 (2014).
65. Di Fede, E. et al. Expanding the phenotype associated to KMT2A variants: overlapping clinical signs between Wiedemann-Steiner and Rubinstein-Taybi syndromes. *Eur. J. Hum. Genet.* **29**, 88–98 (2021).
66. Kim, D., Langmead, B. & Salzberg, S. L. HISAT: a fast spliced aligner with low memory requirements. *Nat. Methods* **12**, 357–360 (2015).
67. Li, H. et al. The sequence alignment/map format and SAMtools. *Bioinformatics* **25**, 2078–2079 (2009).
68. Trapnell, C. et al. Transcript assembly and quantification by RNA-Seq reveals unannotated transcripts and isoform switching during cell differentiation. *Nat. Biotechnol.* **28**, 511–515 (2010).
69. Rossi, F. et al. Circular RNA ZNF609/CKAP5 mRNA interaction regulates microtubule dynamics and tumorigenicity. *Mol. Cell* **82**, 75–89.e79 (2022).

Acknowledgements

We thank all lab members for their critical discussion. This work was supported by grants from the National Key R&D Program of China (2024YFC3405902 and 2021YFA1300503 to L.Y.; 2021YFA1300501 to L.-L.C.), the National Natural Science Foundation of China (NSFC, 32430018 to L.Y.), the CAS Project for Young Scientists in Basic Research (YSBR-009 to L.-L.C.) and the Science and Technology Commission of Shanghai Municipality (STCSM, 23JS1400300 and 23DX1900102 to L.Y.; 23DX1900101 to L.-L.C.). This work has been supported by the New Cornerstone Science Foundation through the New Cornerstone Investigator Program and the XPLOER PRIZE. This work was supported by the Medical Science Data Center in Shanghai Medical College of Fudan University. We also thank the Core Facility of Shanghai Medical College, Fudan University for use of instruments.

Author contributions

L.Y. and L.-L.C. conceived the project. M.C. and S.-M.C. performed experiments with the help of Y.-X.L., C.-X.L., and Y.-F.X., supervised by L.Y. and L.-L.C. G.-H.Y. performed computational analyses, supervised by L.Y. J.W. and Y.-L.G. performed RNA-seq library preparation for deep sequencing, supervised by L.Y. L.Y., L.-L.C., M.C., G.-H.Y., and S.-M.C. wrote the paper with input from all authors. All authors read and approved the manuscript.

Competing interests

L.-L.C. is a scientific co-founder of RiboX Therapeutics. L.Y. and M.C. have filed a patent application (2024119726080) relating to this work through Children's Hospital of Fudan University. The remaining authors declare no competing interests.

Additional information

Supplementary information The online version contains supplementary material available at <https://doi.org/10.1038/s41467-025-63686-7>.

Correspondence and requests for materials should be addressed to Li Yang.

Peer review information *Nature Communications* thanks Kevin Myant and the other anonymous reviewer(s) for their contribution to the peer review of this work. A peer review file is available.

Reprints and permissions information is available at <http://www.nature.com/reprints>

Publisher's note Springer Nature remains neutral with regard to jurisdictional claims in published maps and institutional affiliations.

Open Access This article is licensed under a Creative Commons Attribution-NonCommercial-NoDerivatives 4.0 International License, which permits any non-commercial use, sharing, distribution and reproduction in any medium or format, as long as you give appropriate credit to the original author(s) and the source, provide a link to the Creative Commons licence, and indicate if you modified the licensed material. You do not have permission under this licence to share adapted material derived from this article or parts of it. The images or other third party material in this article are included in the article's Creative Commons licence, unless indicated otherwise in a credit line to the material. If material is not included in the article's Creative Commons licence and your intended use is not permitted by statutory regulation or exceeds the permitted use, you will need to obtain permission directly from the copyright holder. To view a copy of this licence, visit <http://creativecommons.org/licenses/by-nc-nd/4.0/>.

© The Author(s) 2025